Alternative lipid synthesis in response to phosphate limitation promotes antibiotic tolerance in Gram-negative ESKAPE pathogens

Roberto Jhonatan Olea-Ozuna[1], Melanie J. Campbell[2], Samantha Y. Quintanilla[1], Sinjini Nandy[1], Jennifer S. Brodbelt[2], and Joseph M. Boll[1, #]

Affiliations:

[1]Department of Biological Sciences, University of Texas at Dallas, Richardson, TX, USA

[2]Department of Chemistry, University of Texas at Austin, Austin, TX, USA

[#]Corresponding Author:

Email: joseph.boll@utdallas.edu

Short Title: Membrane remodeling in response to phosphate limitation promotes antibiotic tolerance

Keywords: Gram-negative; phospholipid; antibiotic tolerance; aminolipid; membrane; bilayer

Abstract

The Gram-negative outer membrane protects bacterial cells from environmental toxins such as antibiotics. The outer membrane lipid bilayer is asymmetric; while glycerophospholipids compose the periplasmic facing leaflet, the surface layer is enriched with phosphate-containing lipopolysaccharides. The anionic phosphates that decorate the cell surface promote electrostatic interactions with cationic antimicrobial peptides such as colistin, allowing them to penetrate the bilayer, form pores, and lyse the cell. Colistin is prescribed as a last-line therapy to treat multidrug-resistant Gram-negative infections.

Acinetobacter baumannii is an ESKAPE pathogen that rapidly develops resistance to antibiotics and persists for extended periods in the host or on abiotic surfaces. Survival in environmental stress such as phosphate scarcity, represents a clinically significant challenge for nosocomial pathogens. In the face of phosphate starvation, certain bacteria encode adaptive strategies, including the substitution of glycerophospholipids with phosphorus-free lipids. In bacteria, phosphatidylethanolamine, phosphatidylglycerol, and cardiolipin are conserved glycerophospholipids that can form lipid bilayers, particularly in the presence of other lipids. Here, we demonstrate that in response to phosphate limitation, conserved regulatory mechanisms induce alternative lipid production in *A. baumannii*. Specifically, phosphate limitation induces formation of three lipids, including amine-containing ornithine and lysine aminolipids. Mutations that inactivate aminolipid biosynthesis exhibit fitness defects relative to wild type in colistin growth and killing assays. Furthermore, we show that other Gram-negative ESKAPE pathogens accumulate aminolipids under phosphate limiting growth conditions, suggesting aminolipid biosynthesis may represent a broad strategy to overcome cationic antimicrobial peptide-mediated killing.

Author Summary

Gram-negative ESKAPE pathogens, including A*cinetobacter baumannii*, are responsible for a dramatic increase in the morbidity and mortality of patients in healthcare settings over the past two decades. Infections are difficult to treat due to antibiotic resistance and tolerance; however, broadly conserved mechanisms that promote antibiotic treatment failure have not been extensively studied. Herein, we identify an alternative lipid biosynthesis pathway that is induced in phosphate starvation that enables Gram-negative ESKAPE pathogens, including *A. baumannii*, *Klebsiella pneumoniae*, and *Enterobacter cloacae* to build lipid bilayers in the absence of glycerophospholipids, which are the canonical bilayers lipid. Replacement of the anionic phosphate in the lipid headgroup with zwitterionic ornithine and lysine promote survival against colistin, a last resort antimicrobial used against Gram-negative infections. These studies suggest that ESKAPE pathogens can remodel their bilayers with phosphate free lipids to overcome colistin treatment and that aminolipid biosynthesis could be targeted to improve antimicrobial treatment.

73

74 **Introduction**

75 The Gram-negative cell envelope consists of a symmetrical bilayer of
76 glycerophospholipids in the inner membrane, while the outer membrane exhibits an
77 asymmetrical composition, with glycerophospholipids in the periplasmic leaflet and
78 lipopolysaccharide enriched in the outer leaflet (1). The intricate organization underscores
79 the remarkable complexity of bacterial membrane architecture, crucial for microbial survival
80 in various environments. However, under specific stress conditions such as nutrient
81 limitation, temperature fluctuations or exposure to antimicrobial agents, certain bacteria
82 activate alternative lipid biosynthesis pathways or modify existing lipids to adapt and ensure
83 cellular viability (2). One example is aminolipids, which contain amino acid headgroups like
84 lysine, glycine, glutamine, and serine-glycine, with ornithine being the most common (3,4).
85 Ornithine lipids (OLs) are phosphorus-free and found exclusively in bacteria; they are absent
86 in archaea or eukaryotes (5). Their basic structure comprises a 3-hydroxylated fatty acid
87 linked by an amide bond to the α-amino group of ornithine and a second fatty acid attached
88 by an ester bond to the 3-hydroxyl group of the first fatty acid (6). Although OLs are found
89 in both the inner and outer lipid bilayers of Gram-negative bacteria, they are enriched in the
90 outer membrane (7–10). OL biosynthesis is catalyzed by two acyltransferases, OlsB and
91 OlsA, or by the bifunctional acyltransferase OlsF (11–13). In some Gram-negative pathogens
92 such as *Pseudomonas aeruginosa* or *Vibrio cholerae*, OLs are exclusively formed under
93 phosphate limiting conditions (14,15), indicating the presence of a specific regulatory
94 mechanism. The importance of aminolipids transcends basic physiology, especially in the
95 context of antibiotic resistance. ESKAPE pathogens, a group of pathogens that include
96 *Acinetobacter baumannii*, are notorious for their ability to overcome antibiotic treatment and

97 cause hospital-acquired infections (16). Aminolipid synthesis has been implicated in
98 increased bacterial fitness under antimicrobial stress (9,17,18), potentially contributing to
99 pathogen persistence in clinical settings. Additionally, there is a notable relationship between
100 membrane lipid remodeling and resistance to colistin, a last-resort antibiotic that is used
101 against multi-drug resistant Gram-negative infections (19–22). Chemical modifications to
102 the lipid A domain of lipopolysaccharide or enrichment of amino acid-containing
103 glycerophospholipids have been associated with colistin resistance (23–25), highlighting the
104 importance of understanding lipid metabolism in combating antibiotic resistance.

105 In this study, we demonstrate that *A. baumannii* produced two aminolipids in limiting
106 phosphate growth conditions, including lysine lipids (LLs) and OLs. OL and LL synthesis is
107 dependent on the *olsB* and *olsA* genes, and *olsB* expression is regulated transcriptionally by
108 the response regulator, PhoR. Additionally, mutants deficient in aminolipid synthesis exhibit
109 increased colistin susceptibility relative to wild type. We also found that other Gram-negative
110 ESKAPE pathogens, including *Klebsiella pneumoniae* and *Enterobacter cloacae*,
111 accumulate aminolipids under phosphate limited growth conditions. These findings suggest
112 a broad survival strategy among ESKAPE pathogens that could promote survival during
113 antibiotic treatment.
114
115
116
117
118
119
120

121

122 **Results**

123 **Phosphate limitation induces lipid membrane composition modifications in *A.***
124 ***baumannii***

125 The membrane lipid composition of diverse *A. baumannii* isolates was analyzed,
126 including strains ATCC 17978, ATCC 19606, and AB5075, cultivated in complex lysogeny
127 broth (LB) medium supplemented with ^{32}P-orthophosphoric acid. Labelled cells were
128 collected at mid-logarithmic growth phase, lipids were extracted using the Bligh and Dyer
129 method, and separated by hydrophobicity using two-dimensional thin-layer chromatography
130 (TLC), as previously (20,26,27). We also prepared lipid extracts from *Escherichia coli* K-12
131 strain W3110 for comparison, which served as a well-characterized standard (28). TLC
132 analysis showed conserved glycerophospholipid enrichment corresponding to known
133 structures, including phosphatidylethanolamine (PE), phosphatidylglycerol (PG), and
134 cardiolipin (CL) (**Figure S1A**). Additionally, *A. baumannii* strains also produced two distinct
135 lipid species, including lyso-PE (20) and an unknown phospholipid, denoted as UPL1, that
136 could be a CL derivative, mono-lyso CL (29). The chemical structures of known
137 phospholipids are shown in **Figure S1B**.

138 *A. baumannii* strain ATCC 17978 was cultured in minimal medium with either 1 mM
139 (excess) or 50 μM (limiting) phosphate, conditions commonly used to distinguish between
140 phosphate-sufficient and phosphate-limited growth (6, 13–15, 29, 30). Growth in 1 mM
141 phosphate induced a lipid composition almost equivalent to growth in complex LB medium
142 (**Figure 1 and Figure S1A**). One notable change was that UPL1 was absent, and another
143 unidentified lipid, denoted as UPL2, was formed. To explore lipid biosynthesis under
144 phosphate-limiting conditions, membrane lipid profiles were analyzed after growth in

145 minimal media supplemented with 50 µM (limiting) phosphate concentrations (**Figure 1**).
146 Limited phosphate availability impacted relative lipid levels, suggesting decreased
147 phosphate-containing lipid synthesis. However, unlike PE and PG glycerophospholipids,
148 relative CL levels did not change significantly, suggesting its production may provide a
149 strategy to maintain membrane charge stability. Concomitant production of three unknown
150 lipids, referred to as unknown lipids 1 (U1), 2 (U2), and 3 (U3), were produced in phosphate
151 limiting growth. Ninhydrin staining revealed that U1 and U2 contained free amines, like PE.
152 Increased ratios of ninhydrin-stained unknown aminolipids relative to PE showed that under
153 phosphate-limiting conditions, potential phosphate-free aminolipids were produced. The
154 total lipid quantifications after lipids were extracted and separated on TLC is shown in

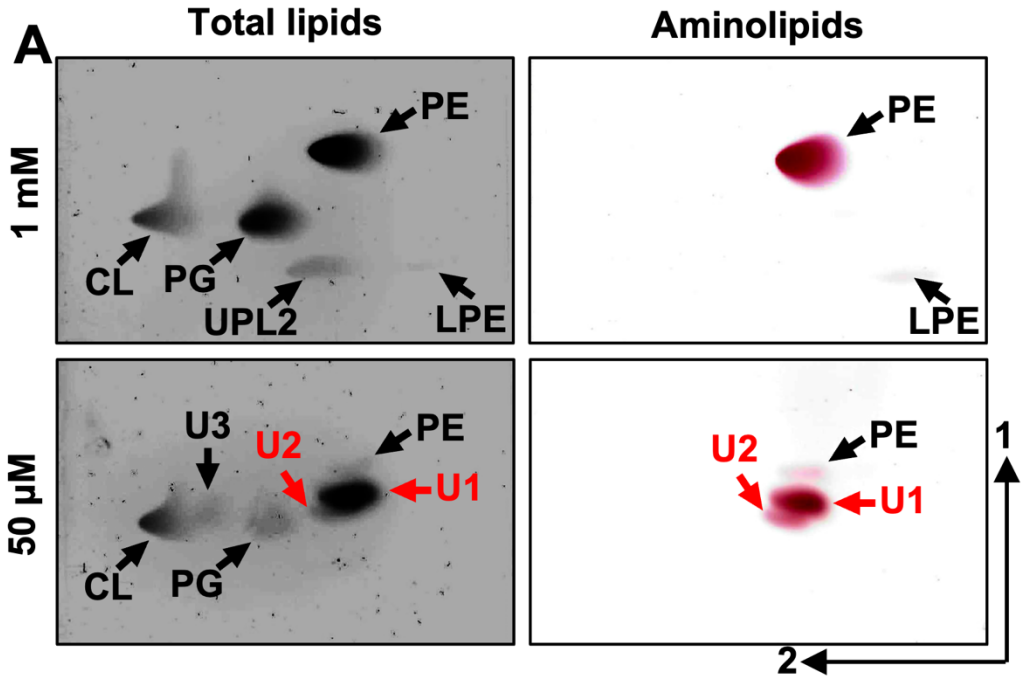

Figure 1: Lipid composition of *A. baumannii* strain ATCC 17978 in excess and limiting phosphate concentrations. Strains were grown in basal media 2 (BM2) with excess (1mM) or limiting (50 µM) phosphate. Cells were collected, lipids were extracted using the Bligh and Dyer method and separated using 2-dimensional thin-layer chromatography. Total lipids were stained with sulfuric acid (left). Aminolipids were stained using ninhydrin (right). Specific lipids are labelled: PE, phosphatidylethanolamine; PG, phosphatidylglycerol; CL, cardiolipin; LPE, lyso-PE; U1, unknown lipid 1; U2, unknown lipid 2; UPL1, unknown phospholipid 1. Red letters denote aminolipids that provide the focus of the study.

155 **Figure S2A**.

156 Growth in limiting phosphate concentrations slowed growth in ATCC 17978 relative
157 to excess phosphate (**Figure S2B**), and microscopic analysis revealed that cells elongated
158 and increased their surface area when phosphate is limiting (**Figure S2C and S2D**), a
159 response previously reported in other Gram-negative bacteria (32). Additionally, while the
160 composition of lipooligosaccharide (LOS) fractions remained consistent across limiting
161 phosphate conditions, the relative level of LOS was decreased under phosphate limitation
162 (**Figure S2E**).
163
164 **Aminolipids synthesized during phosphate limitation are OLs and LLs**
165 One dimensional TLC showed three lipids (PE, U1, and U2) stained with ninhydrin
166 (**Figure S3A**). After separation of lipids based on hydrophobicity, individual bands
167 corresponding with U1 and U2 were scraped from the TLC plates and extracted using the
168 Bligh and Dyer method. U1 and U2 bands were analyzed by liquid chromatography-mass
169 spectrometry (LC-MS) and structurally characterized using tandem mass spectrometry
170 (MS/MS) (**Figure 2**). The elution profiles obtained for the U1 and U2 bands are displayed in
171 **Figures 2A** and **2D,** respectively. To determine the composition of aminolipids, a data-
172 dependent acquisition method was used to isolate and activate the most abundant ions
173 detected in each chromatographic peak with higher energy collisional dissociation (HCD) in
174 negative-ionization mode. HCD of precursor *m/z* 621.52 found in the U1 extract resulted in
175 the loss of the headgroup, which was observed at *m/z* 131.08, and corresponded to
176 deprotonated ornithine (**Figure 2B**). The most abundant fragment ion (*m/z* 367.30) was used
177 to identify the acyl chain connected to the headgroup as 16:0 (number of carbon atoms:
178 double bonds). Further, the complementary ion of *m/z* 253.22 confirmed the identity of the
179 fatty acid connected at the 3-hydroxyl position of the first fatty acid as 16:1. Following this

analysis, lipids containing a double bond were subsequently targeted in a second LC run in the positive-ionization mode using 193 nm ultraviolet photodissociation (UVPD) for MS/MS. UVPD is an alternative fragmentation method that utilizes high-energy photons to activate and dissociate the selected lipid precursor ions, allowing localization of the double bonds within the fatty acyl chains. UVPD of precursor *m/z* 623.53 produced two fragment ions separated by 24 Da that originate from cleavages adjacent to the double bond. This pair of diagnostic ions localizes the double bond to the 9th position (**Figure 2C**). This LC-MS/MS strategy identified 49 OLs, including double bond isomers, and 10 unknown lipids in the U1 extract (**Table S1**) and a total of 24 OLs and 16 unknown lipids in the U2 extract (**Table S2**).

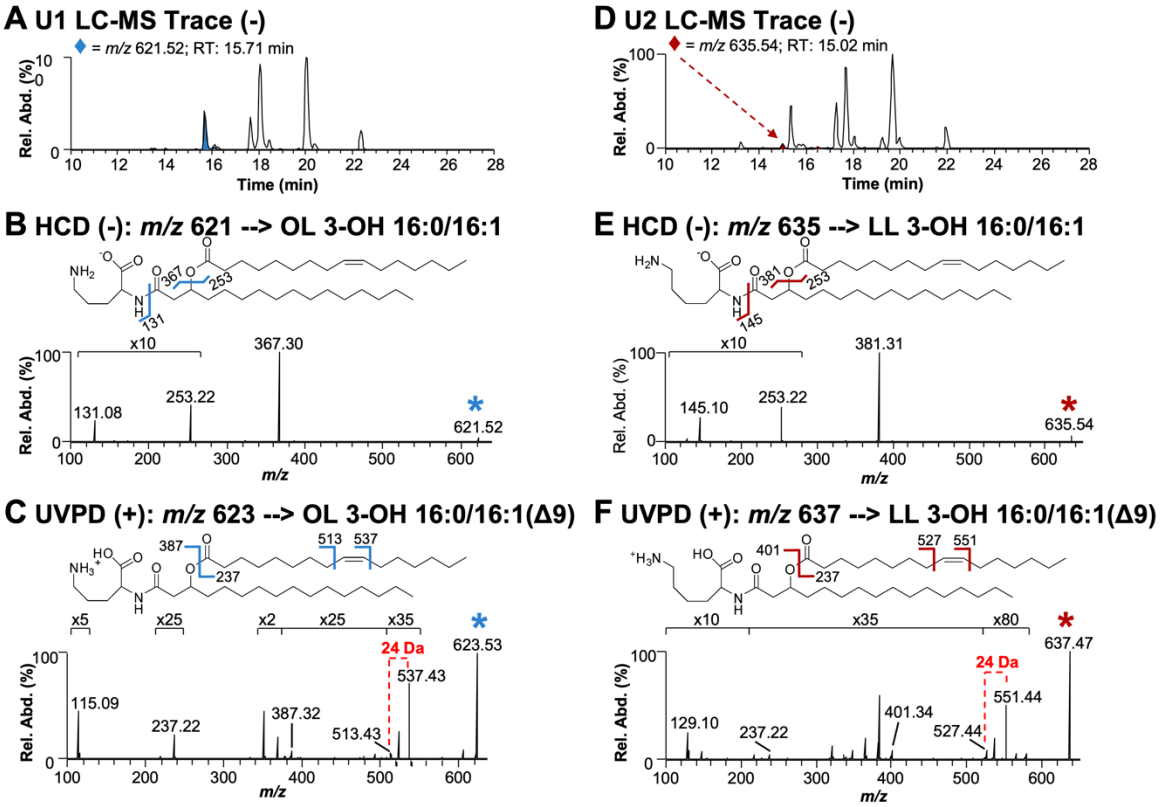

Figure 2: Structural analysis of the lipids produced during phosphate limitation. A. LC-MS trace of U1 lipid extract in negative-ionization mode. **B.** HCD (NCE 22) mass spectrum of *m/z* 621.52 ($[M-H]^-$), an ornithine lipid found in the U1 extract**. C.** UVPD (4 pulses at 2 mJ/pulse) mass spectrum of *m/z* 623.53 ($[M+H]^+$). **D.** LC-MS trace of U2 lipid extract in negative-ionization mode. **E.** HCD (NCE 22) mass spectrum of *m/z* 635.54 ($[M-H]^-$), a lysine lipid found in U2 extract. **F.** UVPD (4 pulses at 2 mJ/pulse) mass spectrum of *m/z* 637.47 ($[M+H]^+$). The selected precursor ions are labeled with asterisks in B, C, E, and F.

189 HCD of the unknown lipids yielded similar fragmentation to that observed for OLs, but the
190 fragmentation patterns were distinguished by the release of a deprotonated headgroup that
191 corresponded to either a lysine or monomethylated ornithine headgroup (*m*/*z* 145.10) (**Figure**
192 **2E**). While the aminolipid head group could be either lysine or monomethylated ornithine,
193 the absence of an ortholog for OlsG, the enzyme responsible for OL methylation (33), and
194 the presence of *olsG* only in certain planctomycete genomes, strongly suggests that OL
195 methylation is unlikely to occur in *A. baumannii*. Therefore, the identified lipid is denoted
196 herein as a LL.

197 After confirming that *A. baumannii* strain ATCC 17978 produces OLs and LLs, we
198 explored if other *A. baumannii* isolates form these aminolipids during phosphate limitation.
199 One-dimensional TLC stained with ninhydrin revealed that diverse *A. baumannii* strains,
200 including ATCC 17978, ATCC 19606, AB5075, AYE, and the environmental isolate, *A.*
201 *baylyi*, were also capable of aminolipid biosynthesis in response to phosphate limitation
202 (**Figure S3B**). Together, these studies suggest that *Acinetobacter* can form lipid bilayers with
203 not only glycerophospholipids, but also membranes enriched with OLs and LLs when
204 phosphate availability is limited.

205

206 **Differentially regulated genes during phosphate starvation**

207 To determine genes that regulate aminolipid biosynthesis, total RNA was isolated,
208 rRNA was depleted, and transcripts were sequenced from *A. baumannii* strain ATCC 17978
209 after growth in minimal media supplemented with 1 mM (excess) and 50 μM (limiting)
210 phosphate. Using a 3-fold cutoff for the weighted proportions fold change and an FDR p-
211 value correction < 0.05, 67 upregulated genes and 109 downregulated genes were found
212 (**Figure 3A**). Many down-regulated genes were involved in iron uptake, such as those coding

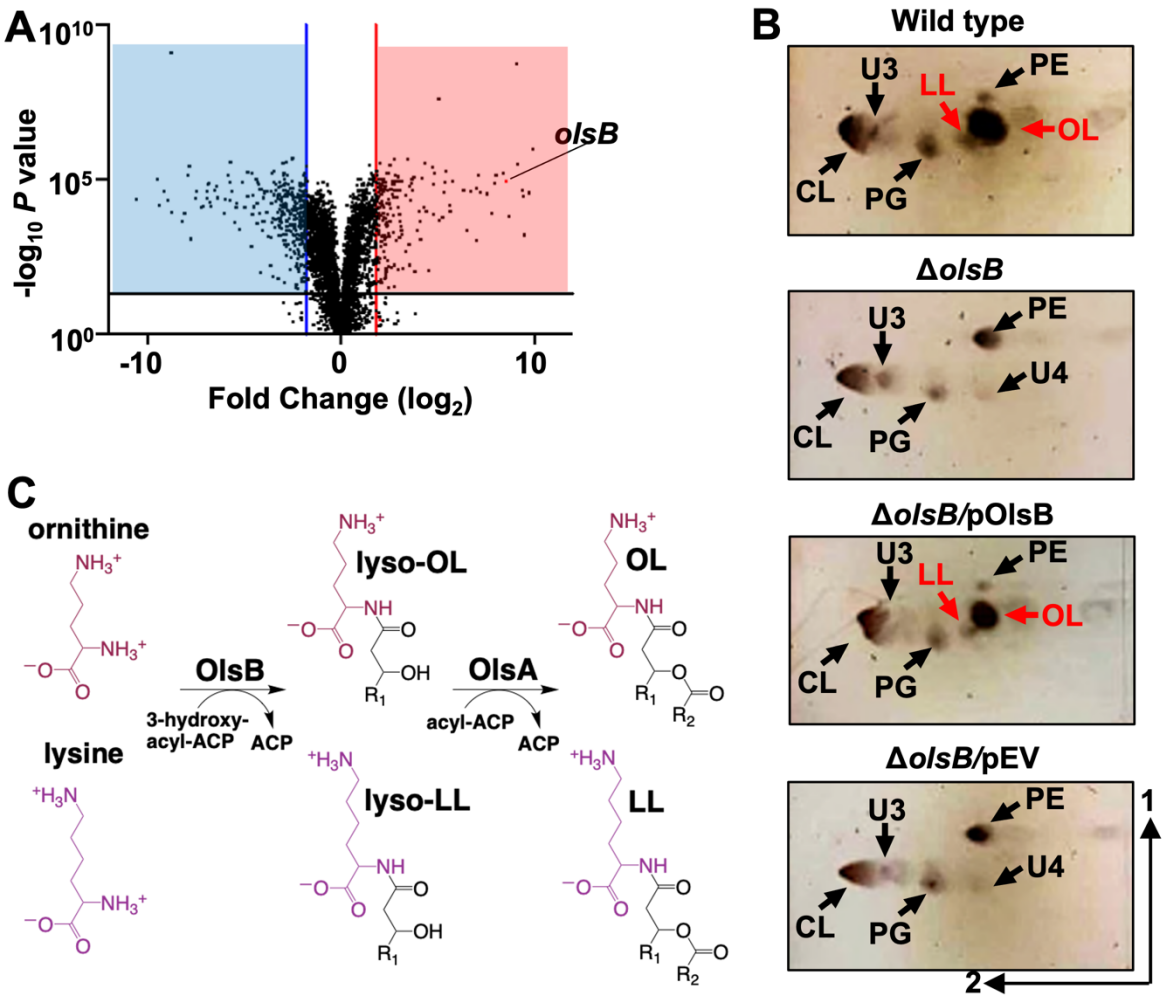

Figure 3: The *olsB* gene is required for ornithine and lysine lipid formation in phosphate limited growth conditions. A. Volcano plot of differentially regulated genes in excess and limiting phosphate. Lines indicate 3.5-fold cutoffs. **B.** 2D thin-layer chromatography stained with sulfuric acid showing wild type and Δ*olsB* strains grown in phosphate limiting (50 µM) conditions. Specific lipids are labelled: PE, phosphatidylethanolamine; PG, phosphatidylglycerol; CL, cardiolipin; OL, ornithine lipid; LL, lysine lipid; U3, unknown lipid 3; U4, unknown lipid 4. OL and LL aminolipids are labelled in red. **C.** Proposed ornithine lipid (OL) and lysine lipid (LL) biosynthesis pathways in *A. baumannii*.

213 for ferric uptake regulators (Fur) and components of the ABC transporters for iron.
214 Additionally, genes involved in lysine degradation and aminoacid metabolism were down-
215 regulated, indicating potential changes in nitrogen metabolism under phosphate-limited
216 conditions. Upregulated genes were associated with TAT-dependent proteins export, which
217 could be involved in the transport of key lipids or membrane proteins, as well as
218 phospholipases, which may play a role in membrane remodeling. Furthermore, genes related

219 to regulation and phosphate transporters were induced, likely in response to changes in
220 phosphate availability. A complete list of significant ($P < 0.05$) up- and down-regulated genes
221 is included in **Table S3**. The RNA-sequencing results were validated using qRT-PCR
222 analysis to measure differential expression between three specific genes in excess and
223 limiting phosphate concentrations (**Figure S4A**) and via phenotypic characterization of
224 several mutants described below. Validation of the dataset suggested that phosphate
225 limitation induces a broad transcriptional reprogramming, affecting processes such as lipid
226 biosynthesis, membrane integrity, and nutrient uptake, which are crucial for bacterial survival
227 under stress conditions.

228 One notable up-regulated gene (*A1S_0889*) showed a $\log_2$ fold change of 8.57 and
229 31% identity and 51% similarity (91% coverage) to *P. aeruginosa olsB*. While not induced
230 in phosphate starvation, *A. baumannii* also encodes a putative *olsA* orthologue (*A1S_2990*)
231 with 43% identity and 61% similarity (78% coverage) to *P. aeruginosa olsA*. OlsBA has been
232 characterized in several bacteria and is involved in OLs biosynthesis (8,11,12,14,34).
233 Notably, *A. baumannii olsA* is located at a distinct site on the chromosome relative to *olsB*
234 and is not transcriptionally regulated by phosphate concentrations.

235

236 ***olsB* and *olsA* genes are required for aminolipids synthesis in *A. baumannii***

237 Differential gene expression analysis indicated changes in gene dosage in response to
238 excess/limiting phosphate concentration. Specifically, *A1S_0889* expression increased in
239 response to phosphate limitation, whereas *A1S_2990* expression did not change. To confirm
240 that *A1S_0889* was an *olsB* orthologue, we generated Δ*olsB* in *A. baumannii* strain ATCC
241 17978, by deleting codons 34 and 214. TLC analysis revealed that under phosphate

242 limitation, aminolipids were absent in the *olsB*-deficient mutant and a mutant carrying only
243 the empty vector but wild-type accumulated OLs and LLs (**Figure 3B**). Furthermore, *olsB*
244 complementation from a non-native promoter restored OL and LL formation. Based on the
245 lipid migration patterns in wild type, the lipids are OLs and LLs.

246 Additionally, we generated Δ*olsB* (*HMPREF0010_01383*) using recombineering in
247 strain ATCC 19606 and also analyzed the *olsB::tn* and *olsA::tn* mutants from the AB5075
248 transposon mutant library (35), which contain insertions in the respective genes,
249 *ABUW_3039* and *ABUW_0502*. Lipid analysis when the mutants were cultivated under
250 phosphate limitation showed that the wild-type strains ATCC 19606 and AB5075 produced
251 OLs and LLs, while the *olsB* and *olsA* mutants did not (**Figure S4B and S4C**). The *olsA*::*tn*
252 mutant lipid profile did not show the expected accumulation of lyso-aminolipids, consistent
253 with findings in other Gram-negative Δ*olsA* mutants (30). This suggests that lyso-aminolipids
254 are tightly regulated and rapidly degraded within the cell. These data suggested that ornithine
255 and lysine lipid biosynthesis in *A. baumannii* is dependent on OlsB and OlsA. We will also
256 note that we observed an unknown lipid, labelled as U4 in figure 3B and figure S4B that may
257 indicate an OlsA-dependent lipid.

258 Together, the data supports a model suggesting that aminolipid synthesis occurs in at
259 least two distinct steps within *A. baumannii* (**Figure 3C**), consistent with previous work in
260 other Gram-negative bacteria (11,12). Initially, ornithine and lysine undergo acylation in an
261 OlsB-dependent reaction, leading to the formation of lyso-OL and lyso-LL. Subsequently, in
262 a second step facilitated by OlsA, lyso-OL and lyso-LL are further acylated at the hydroxy
263 position, yielding OL and LL, respectively.

264 Microscopic analysis and comparison of LOS fractions and levels between
265 aminolipid-producing and aminolipid-deficient *A. baumannii* strains revealed no significant
266 morphological differences (**Figure S4D and S4E**) or changes in LOS fractions and relative
267 levels (**Figure S2E)**. However, it is noteworthy that the core fraction of LOS from *A.*
268 *baumannii* strains ATCC 19606 differs from of the ATCC 17978 or AB5075 strains.
269 Additionally, a faint band in the core fraction was observed in the *olsA*::*tn* transposon mutant
270 of AB5075, which was not present in the wild type strain.
271
272 **Mutants deficient in aminolipids synthesis show differential growth rate under**
273 **phosphate limitation**
274 To assess growth rates under phosphate limitation, wild-type and *olsB* mutant strains
275 were grown in minimal medium with limiting phosphate concentrations (**Figure S4F**). The
276 optical density at 600 nm (OD_{600}) was monitored over time. While growth of strain ATCC
277 17978 Δ*olsB* was not impacted, the growth rate in strains ATCC 19606 and AB5075 was
278 reduced in the *olsB* or *olsA* T101 mutants, suggesting there are strain-dependent effects on
279 aminolipid biosynthesis that impact fitness.
280
281 **Aminolipid biosynthesis mutants are defective in colistin tolerance**
282 Changes in lipid composition could alter the physicochemical properties of the
283 bilayers, particularly the charge. To explore this concept, the impact of aminolipids
284 biosynthesis on colistin tolerance was measured in *A. baumannii* strain ATCC 17978, where
285 growth rate was not impacted in the *olsB* mutant (**Figure S4F**). Colistin is a cyclic peptide
286 that directly engages with the negative membrane charge, while the hydrophobic tail forms

287 pores, leading to bactericidal activity. Colistin is a last resort antibiotic used against multidrug
288 resistant Gram-negative bacterial infections. Our studies indicate increased colistin
289 susceptibility in the *olsB*-deficient mutant relative to the wild-type strain (**Figure 4A and**
290 **Figure S5A**), suggesting the antibiotic could be more effective against *A. baumannii* when
291 aminolipid biosynthesis is inhibited. Under high phosphate conditions, the membrane lipid
292 composition remains typical of standard bacterial membranes, resulting in higher relative
293 colistin susceptibility (Figure 4C). However, in phosphate limited conditions, lipid turnover

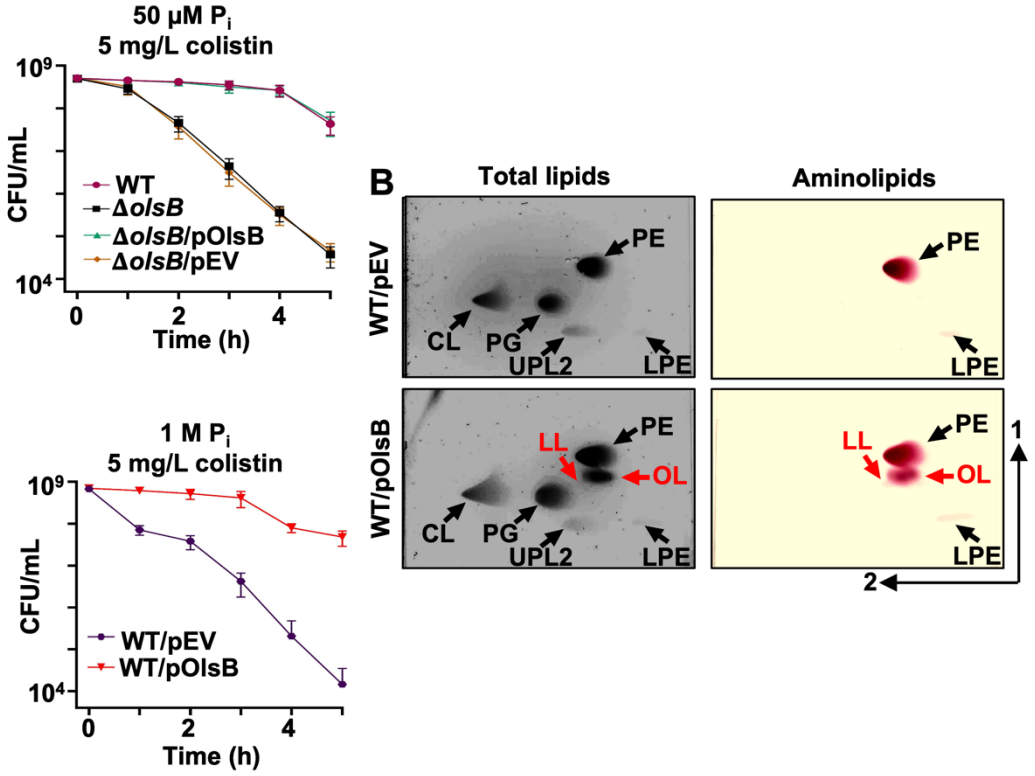

Figure 4: Aminolipids promote colistin tolerance in *A. baumannii*. A. Colistin-dependent killing in wild type and Δ*olsB* mutant strains under phosphate limitation ($n = 3$). Error bars indicate standard deviation. Wild type (WT) strains carrying pOlsB or empty vector were subjected to 5 mg/L colistin exposure over time. CFU/mL were calculated every 0.5 h. **B.** Total lipids were extracted using the Bligh and Dyer method and separated using 2D thin-layer chromatography. Lipids were stained with sulfuric acid (left). Aminolipids were stained using ninhydrin (right). Specific lipids are labelled: PE, phosphatidylethanolamine; PG, phosphatidylglycerol; CL, cardiolipin; LPE, lyso-phosphatidylethanolamine; LL, lysine lipid; OL, ornithine lipid; U3, unknown lipid 3. OL and LL are labelled in red. **C.** Colistin-dependent kill curves (left) and growth rate analysis (right) in wild type expressing empty vector (pEV) or pOlsB under high phosphate conditions ($n = 3$). Error bars indicate standard deviation.

294 increases, leading to the replacement of phospholipids with non-phosphorylated aminolipids,
295 which probably contributes to enhanced colistin tolerance. Overexpression of *olsB* in wild-
296 type *A. baumannii* was sufficient to produce aminolipids during cultivation in excess
297 phosphate (**Figure 4B**). Analysis demonstrated that *olsB* induction led to increased colistin
298 tolerance (**Figure 4C and Figure S5B**). Therefore, OlsB-dependent aminolipid biosynthesis
299 in *A. baumannii* promotes colistin tolerance, a last-line antibiotic for combating multidrug-
300 resistant Gram-negative bacteria.
301

302 **PhoR regulates aminolipid biosynthesis in *A. baumannii***

303 Previous work established that aminolipid production generally occurs in response to
304 phosphate limitation (6,14,15,36,37). Consequently, we expected to find a Pho box upstream
305 of the putative *olsB* gene. Using the *E. coli* pho box consensus sequence (38), a putative Pho
306 box was identified that precedes the *olsB* gene in diverse *Acinetobacter* isolates, including

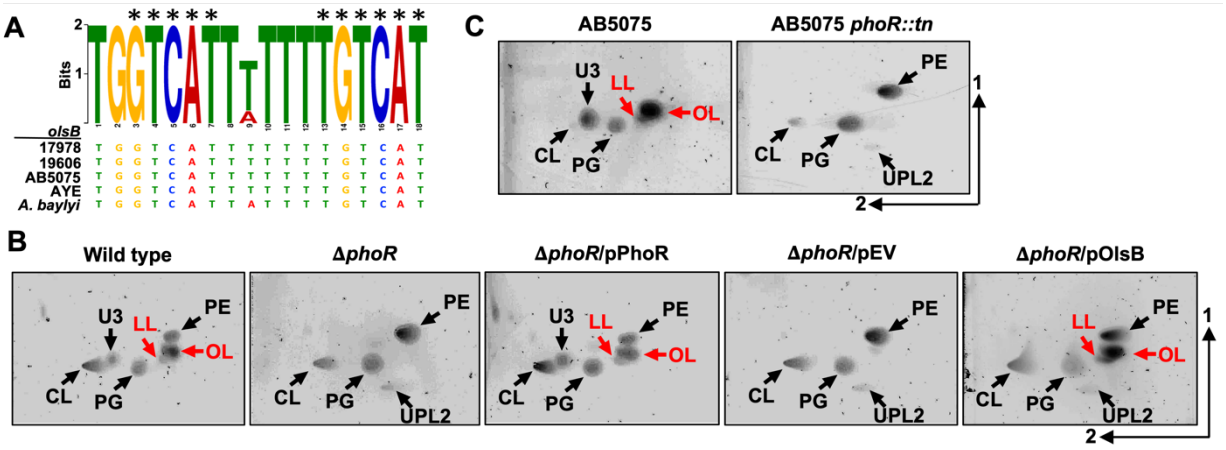

Figure 5: PhoR regulates *olsB* gene expression and aminolipid formation in *A. baumannii* strains. **A.** Predicted Pho box sequence alignments from *A. baumannii* strain 17978, 19606, AB5075, AYE, and *A. baylyi olsB* promoters. Black asterisks represent conserved nucleotides in the *E. coli* Pho box consensus (CT*GTCAT*NNNNC*TGTCAT*). **B.** 2D thin-layer chromatography lipid analysis from *A. baumannii* strain ATCC 17978 wild type and mutants grown in minimal media supplemented with 50 µM (limiting) phosphate. **C.** 2D thin-layer chromatography lipid analysis from *A. baumannii* strain AB5075 wild type and the *phoR* Tn*26* mutant in minimal media supplemented with 50 µM (limiting) phosphate. Lipids were stained with sulfuric acid. OL and LL aminolipids are labelled in red.

307 ATCC 17978 (**Figure 5A**), but not preceding the *olsA* gene. The identified Pho box shows
308 significant sequence similarity to the *E. coli* consensus (CT*GTCAT*NNNNC*TGTCAT*), with
309 conserved nucleotides present in multiple *Acinetobacter* strains, including *A. baumannii*
310 strains ATCC 17978, 19606, AB5075, AYE, and *A. baylyi*. These results are consistent with
311 our transcriptomics analysis, which also suggested *olsA* gene expression is not responsive to
312 phosphate concentrations.

313 Phosphate sensing and diverse responses are regulated by the two-component system,
314 PhoB/PhoR, in many bacteria (39). When phosphate levels decrease, the sensor kinase, PhoR,
315 becomes activated, leading to autophosphorylation. Subsequent phosphotransfer to the
316 cognate response regulator, PhoB results in a conformational change and DNA binding (40)
317 at target promoters to induce gene expression.

318 These findings imply that the PhoB/PhoR two-component system regulates OL and
319 LL biosynthesis in *A. baumannii* through *olsB* expression. To validate this hypothesis, we
320 generated Δ*phoR* (*A1S_3376*) in *A. baumannii* ATCC 17978 by deleting codons 66 to 409.
321 Lipid analysis after growth limiting phosphate, showed that the Δ*phoR* mutant accumulates
322 glycerophospholipids PE, PG, CL, and UPL2, while failing to synthesize OL, LL, and U3,
323 unlike the wild-type strain (**Figure 5B**). Complementation of the *phoR*-deficient mutant with
324 the PhoR allele restored OL and LL formation, while aminolipids were absent in the mutant
325 carrying the empty vector. Expression of *olsB* from a non-native promotor in the Δ*phoR*
326 mutant restored OL and LL biosynthesis. Additionally, we examined the lipid patterns of the
327 *phoR* (*ABUW_0105*)-transposon mutant of *A. baumannii* AB5075 grown under phosphate
328 limitation (**Figure 5C**). Lipidomic analysis revealed that, unlike the wild-type strain, the
329 *phoR::tn* mutant predominantly accumulated phospholipids and was unable to produce OL

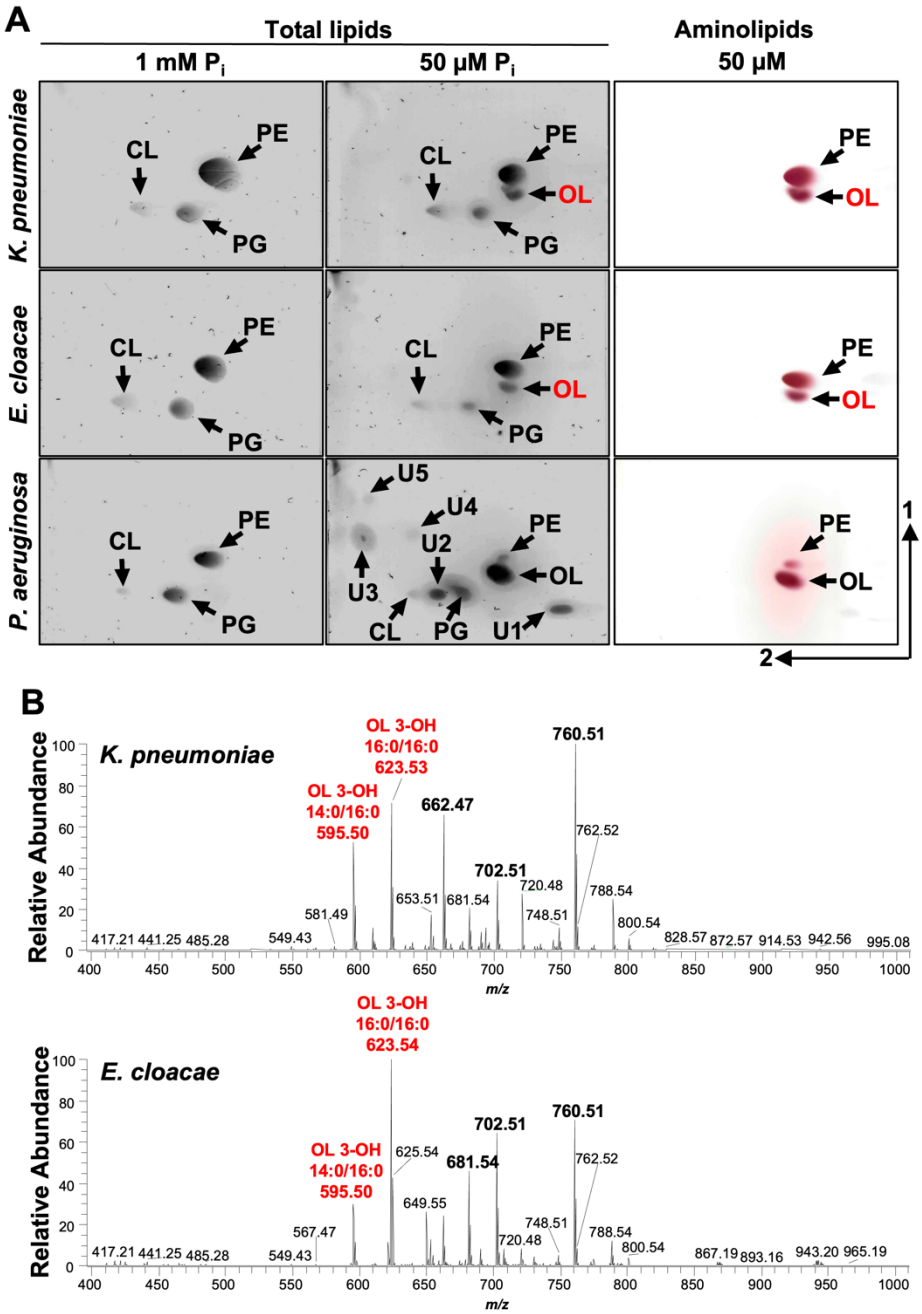

Figure 6: Aminolipid biosynthesis is conserved in Gram-negative ESKAPE pathogens. 2D thin-layer chromatography of lipids extracted from wild type *K. pneumoniae* strain KPNIH1, *E. cloacae* strain ATCC 13047, and *P. aeruginosa* strain PAO1 grown in excess (1 mM) or limiting (50 μM) phosphate conditions. Totals lipids were stained with sulfuric acid (left). Aminolipids were stained using ninhydrin (right). Specific lipids are labelled: PE, phosphatidylethanolamine; PG, phosphatidylglycerol; CL, cardiolipin; OL, ornithine lipid; U1, U2, U3, U4, and U5; unknown compounds 1, 2, 3, 4, and 5. **B.** Representative MS1 spectra from shotgun analysis of animolipids isolated from *K. pneumoniae* ($n = 3$) and *E. cloacae* ($n = 3$). The five most enriched lipids are bolded, including two ornithine lipids (OL), labelled in red.

330 or LLs. Together, these findings suggest that *olsB* expression in *A. baumannii* is mediated by

331 the *phoR* regulatory gene.

332

333 **Other Gram-negative ESKAPE pathogens form aminolipids under conditions of**
334 **phosphate depletion**

335 In addition to *P. aeruginosa* (14), *A. baumannii* is the second Gram-negative
336 ESKAPE bacterium where the OL biosynthesis has been described using a OlsBA-dependent
337 mechanisms. Uniquely, *A. baumannii* also produces LL via the same pathway. These findings
338 prompted us to investigate if other Gram-negative ESKAPE pathogens, such as *Klebsiella* or
339 *Enterobacter*, are also capable of aminolipid biosynthesis under phosphate limitation. TLC
340 analysis of total lipids from *K. pneumoniae*, *E. cloacae* or *P. aeruginosa* after growth in
341 minimal medium supplemented with excess phosphates showed production of the canonical
342 membrane phospholipids PE, PG, and CL (**Figure 6A**). However, when cultivating *P.*
343 *aeruginosa* in phosphate limitation (50 μM), a significant decrease in relative phospholipid
344 levels was observed, and the synthesis of five unknown compounds and OL was induced. *K.*
345 *pneumoniae* and *E. cloacae* cultivated in low phosphate concentrations (50 μM), also showed
346 decreased levels of phospholipid production and accumulation of an unknown lipid. The
347 unknown lipid exhibited a migration pattern and ninhydrin staining on TLC like OL,
348 suggesting that aminolipid biosynthesis may be a conserved response to phosphate limiting
349 growth conditions that could promote tolerance to antibiotics in Gram-negative ESKAPE
350 pathogens.

351 To confirm the putative OL identity, total lipids were extracted using the Bligh and
352 Dyer method after cells were grown in 50 μM phosphate. 1-D TLC (**Figure S6**) on total lipids
353 stained with ninhydrin showed two prevalent lipids (lane 1). The band corresponding to OLs
354 was scraped from the plate and extracted. Extracted lipids from three replicates were run on

355 1-D TLC showing enrichment of the putative OL relative to PE. Negative-ionization mode
356 MS1 shotgun analysis on the purified lipids showed five enriched lipids in each strain
357 (**Figure 6B**). MS/MS analysis of the lipids present in *K. pneumoniae* sample revealed two
358 ornithine lipids (*m/z* 595.50 and 623.53), two PE lipids (*m/z* 662.47 and 702.51), and a *m/z*
359 consistent with phosphatidylthreonine (*m/z* 760.51) (**Table S4**). Spectra from the *E. cloacae*
360 lipid analysis included two ornithine lipids (*m/z* 623.54 and 595.50), PE (*m/z* 702.51), a *m/z*
361 consistent with phosphatidylthreonine (*m/z* 760.51), and an unknown lipid that may be a
362 modified OL (*m/z* 681.54) (**Table S5**). Together the migration of the lipids via 2-D TLC and
363 the MS analysis provide strong complementary evidence that growth in limiting phosphate
364 results in alternative synthesis of OLs.
365
366 **Discussion**
367 Bacteria have evolved various regulatory mechanisms to sense and adapt to
368 environmental stress. Here, we show that under phosphate-limiting conditions, *A. baumannii*
369 produces ornithine and lysine lipids through regulated expression of *olsB*. The aminolipids
370 alter the lipid bilayer composition to promote tolerance to colistin, an antimicrobial peptide
371 used to treat Gram-negative bacterial infections. Specifically, aminolipids could reduce the
372 electrostatic potential for cationic antimicrobial peptides such as colistin to target the cell,
373 emphasizing changes in bilayer charge as an adaptive mechanism for *A. baumannii* in
374 challenging environments. Although aminolipids are not directly exposed on the membrane
375 surface, their accumulation in the inner leaflet of the outer membrane may alter the overall
376 membrane dynamics, such as lipid packing and membrane fluidity, contributing to enhanced
377 membrane stability and colistin tolerance. Broadly, cell membrane lipid modifications are
378 vital for bacterial survival upon exposure to antimicrobial cationic peptides. For example, *V.*

379 *cholerae* modifies lipid A with glycine or diglycine residues to resist cationic antimicrobial
380 peptides (41). Similarly, other Gram-negative bacteria modify their lipid A structures to resist
381 polymyxins. For instance, *P. aeruginosa* and *A. baumannii* can add positively charged amino
382 groups, such as ethanolamine to lipid A, reducing to overall negative charge and decreasing
383 the binding affinity of polymyxin (20). *K. pneumoniae* and *Enterobacter* species have been
384 shown to add 4-amino-4-deoxy-L-arabinose (L-Ara4N) to lipid A, further neutralizing the
385 negative charge and conferring resistance (21). Similar strategies are employed by various
386 bacterial species, such as *P. aeruginosa*, *Rhizobium tropici*, *Staphylococcus aureus*,
387 *Mycobacterium tuberculosis*, and *Bacillus subtilis*, which modify phospholipids like PG by
388 adding amino acids like lysine or alanine, thereby conferring polymyxins resistance
389 (36,37,42–44).

390 Membrane lipid remodeling during growth under phosphate limitation is a conserved
391 strategy across bacteria, involving the substitution of phospholipids with phosphorus-free
392 lipids alternatives like aminolipids (45). Interestingly, other bacteria, such as *P. aeruginosa*,
393 also modify their lipid composition in response to phosphate limitation (14). Under these
394 conditions, *P. aeruginosa* incorporates OL, replacing phospholipids in the membrane. This
395 remodeling likely ensures that the membrane remains functional and stable despite the
396 phosphate scarcity, highlighting a similar strategy employed by various bacterial species to
397 adapt to nutrient stress. These findings further support the idea the replacement of
398 phospholipids with amino acid-derived lipids, such as ornithine, represents an adaptive
399 mechanism to phosphate limitation, suggesting that this process may be widely conserved
400 across Gram-negative bacteria. While the synthesis of these lipids is not directly induced by
401 the presence of polymyxins, tolerance to polymyxins is an indirect consequence of lipid
402 membrane remodeling, leading to significant changes in membrane chemical properties. The

403 alteration could reduce the net negative charge of the membrane, thereby decreasing CAMP
404 susceptibility.

405 The *olsB* gene is required for OL biosynthesis, but unlike other OlsB-dependent
406 pathways, it also induces LL formation in *A. baumannii*, suggesting metabolic plasticity
407 within the species. Comparing our findings with observations in other bacteria, such as the
408 soil bacterium *Rhodobacter sphaeroides*, which not only produces OLs but also synthesizes
409 glutamine lipids (GLs) (46), further highlights the metabolic diversity in aminolipid
410 biosynthesis. Additionally, recent research has shown that marine bacteria *Ruegeria*
411 *pomeroyi* encode two *olsB* paralogs, one responsible for forming OLs and the other for GLs
412 (30). Although these bacteria inhabit vastly different environments, the similarities suggest
413 that the ability to use multiple substrates for aminolipid synthesis may be a common survival
414 strategy in variable environmental conditions.

415 The transcriptomic analysis uncovered insights into different expression patterns of
416 the *olsB* and *olsA* genes in response to phosphate limitation. Specifically, overexpression of
417 the *olsB* gene was observed during phosphate limited growth, indicating a regulatory
418 mechanism. However, *olsA* expression remained unchanged. The predicted Pho box in the
419 promoter region of *olsB* suggested that the PhoB/PhoR two-component system regulates *olsB*
420 under phosphate limitation conditions. The absence of a Pho box-like motif in the promotor
421 region of *olsA*, in contrast to *olsB*, suggests that *olsA* is regulated by factors distinct from
422 those controlling *olsB* under phosphate limiting conditions. This was confirmed by RNA
423 sequencing (**Figure 3A**) and RT-PCR analysis (**Figure S4A**), which both showed that *olsA*
424 expression remains unchanged in response to phosphate limitation, indicating that its
425 expression is likely controlled by other regulatory mechanisms or constitutive. Consequently,
426 *olsA* is not constitutively expressed under these conditions, but rather its regulation appears

427 to be independent of phosphate availability. The absence of a similar motif in the promoter
428 region of *olsA* implies the influence of other regulatory factors on its expression, independent
429 of phosphate availability. Furthermore, *olsB* overexpression with non-native promoter in *A.*
430 *baumannii* during cultivation in excess phosphate resulted in aminolipid formation,
431 suggesting OlsA-dependent activity occurs after OlsB has formed a lyso-aminolipid. The
432 differential regulatory events may also suggest that OlsA utilizes other substrates. For
433 instance, in *Rhodobacter capsulatus*, OlsA functions as a bifunctional enzyme, active in both
434 OL and phosphatidic acid biosynthesis (47). Additionally, we confirmed the role of the *phoR*
435 gene as a key regulator in aminolipid biosynthesis in *A. baumannii*, highlighting its fine-
436 tuned regulation in response to environmental stressors such as phosphate limitation.
437 Interestingly, this regulatory mechanism shares similarities with species like *Sinorhizobium*
438 *meliloti* or *V. cholerae*, where PhoB/PhoR also regulates OLs synthesis under phosphate
439 limitation conditions (6,15), underscoring the evolutionary conservation of these adaptive
440 mechanisms across different bacterial taxa.

441 Finally, the presence of *olsB* and *olsA* orthologues in *A. baumannii* raises questions
442 about the diversity of aminolipid biosynthesis pathways among pathogens. Interestingly,
443 bacteria such as *Klebsiella* and *Enterobacter* lack these orthologs, suggesting distinct
444 biosynthesis pathways compared to *A. baumannii*. This absence prompts further investigation
445 into alternative pathways or genes involved in aminolipid synthesis and their implications
446 for antibiotics resistance and environmental adaptation.

447

448 **Conclusion**

449 The study highlights the impact of phosphate limitation on lipid membrane
450 composition in *A. baumannii*, resulting in the synthesis of OLs and LLs through regulated

451 *olsB* gene expression. Aminolipids can promote tolerance to colistin, an important last-line
452 antimicrobial. These results also underscore the role for *phoR* gene in regulating aminolipid
453 synthesis in *A. baumannii* and show that other Gram-negative ESKAPE pathogens produce
454 aminolipids under phosphate-depleted conditions. Aminolipid biosynthesis is a common
455 adaptive response to phosphate limitation, which could promote pathogen survival both in
456 hospital environment and within the host.
457

458 **Materials and methods**

459 **Bacterial strains and growth.** All strains and plasmids used in this study are listed in **Table**
460 **S6** in the supplemental material. *E. coli*, *Acinetobacter* strains, *K. pneumoniae*, *E. cloacae* or
461 *P. aeruginosa* were initially cultured from frozen stocks on Luria-Bertani (LB Miller) agar
462 at 37ºC. Isolated colonies were used to inoculate LB Miller broth or minimal medium (Tris
463 minimal succinate [TMS]) (31); supplemented with different phosphate concentrations at
464 37ºC. The minimal medium included: Na-succinate 20 mM, NaCl 200 mg/mL, NH_4Cl 450
465 mg/mL, $CaCl_2$ 200 mg/mL, KCl 200 mg/mL, $MgCl_2$ 450 mg/mL, $FeCl_2$ 10 mg/L, and $MnCl_2$
466 10 mg/L, with 10 mM 4-(2-hydroxyethyl)-1-piperazineethanesulfonic acid (HEPES) buffer
467 used at pH 7.2. Na_2HPO_4 was then added to achieve a final concentration of 1 mM (excess)
468 or 50 µM (limiting). All components were dissolved in deionized water and sterilized by
469 filtration trough 0.22 µm pore-size filters and dissolved deionized H_2O. To generate growth
470 curves, overnight cultures of *A. baumannii* strains were diluted to an OD_{600} of ~0.05 in 5 mL
471 of medium, then incubated in glass test tubes at 37ºC for 24 hours. Growth curve data were
472 analyzed and plotted using GraphPad Prism software.

473 *A. baumannii* strain ATCC 17978 has been shown to be a mixture of two variants
474 (48). Colony PCR using primers specific to the cardiolipin synthase gene (*clsC2*) resulted in

475 a PCR product, indicating this study was specific to only the *A. baumannii* 17978 UN variant.
476 *A. baumannii* strains AB5075 and ATCC 19606 have been shown to produce colonies with
477 two opacity phenotypes that are phase variable (49). Microscopic examination showed a
478 majority of opaque forms in strains AB5075 and ATCC 19606 with only 2-3 translucent
479 colonies out of > 200 colonies found on each plate (n = 3 for each strain). The strain ATCC
480 19606 Δ*olsB* and strain AB5075 *olsB::tn* and *olsA::tn* mutants were also examined, but only
481 included opaque variants.
482
483 **Construction of mutant and complementation *A. baumannii* strains.** The primers utilized
484 in this study are listed in **Table S7** in the supplementary material. Genetic mutants of *A.*
485 *baumannii* were generated following established protocols (50–53). Briefly, *A. baumannii*
486 carrying the pMMB67EH^{TetR} plasmid containing the REC$_{Ab}$ coding sequences was diluted
487 from an overnight culture into LB Miller broth containing 10µg/mL of tetracycline at an
488 OD_{600} of ~0.05 and incubated for 45 minutes. REC$_{Ab}$ expression was induced by adding 2
489 mM IPTG, and cells were cultured at 37ºC until they reached mid-log growth phase (OD_{600}
490 of ~0.4). After washing the cells three times in ice-cold 10% glycerol, 10^{10} cells were
491 electroporated in a 2-mm cuvette at 1.8 mV with 5 µg of a recombineering linear PCR
492 product. Subsequently, the cells were cultured for 4 hours in 4 mL of LB Miller broth with 2
493 mM IPTG and then plated on LB agar supplemented with 20 µg/mL of kanamycin. Mutations
494 were validated using PCR.
495 To cure isolated mutants of the pMMB67EH^{TetR}::REC$_{Ab}$ plasmid after mutant
496 isolation, strains were streaked for isolated colonies on LB Miller agar supplemented with 2
497 mM $NiCl_2$ to select cells that had lost the tetracycline cassette (51–54). Cured insertion

498 mutants were then electroporated with pMMB67EH^{TetR} carrying the FLP recombinase. Cells
499 were recovered for 1 hour in 5 mL of LB Miller broth and plated on LB agar containing
500 10µg/mL of tetracycline and 2 mM IPTG to induce expression of the FLP recombinase.
501 Excision of the kanamycin cassette was confirmed by PCR.

502 To complement the *A. baumannii* ATCC 17978 mutants, the coding sequence from
503 *A1S_0889* (*olsB*) was cloned into the KpnI/SalI sites, while the coding sequence from
504 *A1S_3376* (*phoR*) was cloned into the KpnI/BamHI sites in pMMB67EH^{KanR}. Plasmids were
505 expressed in the respective mutants, and all strains were grown in 30 µg/mL of kanamycin
506 and 1 mM IPTG for expression.

507

508 **Analysis of total lipids and aminolipids.** Overnight cultures were used to inoculate 10 mL
509 minimal medium 1 mM phosphate, or 20 mL minimal medium 50 µM phosphate to achieve
510 an OD_{600} of ~0.05, and then incubated for 24 hours at 37 ºC. After the incubation period,
511 cells were collected by centrifugation. Lipids were extracted using the Bligh and Dyer (1959)
512 method (55). The chloroform phase was separated into the individual components on high-
513 performance TLC silica gel plates. For one-dimensional TLC analysis, the plates were
514 developed with chloroform-methanol-water (130:50:8 v/v) mixture. For two-dimensional
515 TLC analysis, a chloroform-methanol-water (140:60:10 v/v) mixture was used in the first
516 dimension and chloroform-methanol-acetic acid (130:50:20 v/v) mixture was used in the
517 second dimension. Lipids on TLC were visualized by treating the plates with 10% sulfuric
518 acid in ethanol at 150ºC (total lipids) or 0.2% ninhydrin in acetone at 100ºC (aminolipids).
519 Lipid quantifications were done using ImageJ software to detect spots above background.
520 Each experiment was independently replicated three times, one representative data set was
521 reported in the quantification, and one representative image was included..

522

523 **Analysis of ^{32}P-labeled phospholipids.** Overnight cultures were diluted to an OD_{600} of ~0.05
524 in 10 mL LB Miller broth supplemented with 5 µCi/mL ^{32}P ortho-phosphoric acid
525 (PerkinElmer) and grown until reaching an OD_{600} of ~0.6. After harvesting the cells, lipid
526 extraction was performed using Bligh and Dyer method (55), followed by analysis using TLC
527 as previously described. Subsequently, the TLC plates were dried, exposed to a
528 phosphorimaging screen, and scanned using an Amersham Typhoon laser scanner.

529

530 **Shotgun Mass Spectrometry:** Dried lipid content from Bligh and Dyer extracted TLC bands
531 of *E. cloacae* WT and *K. pneumoniae* WT biological replicates were solubilized in
532 chloroform and resuspended in methanol: isopropanol (1:1) at a concentration of 200 µM.
533 Shotgun analysis was performed in negative-ionization mode on a Thermo Scientific
534 Orbitrap Fusion Lumos Tribrid mass spectrometer. Nanoelectrospray ionization was
535 performed using Pd/Au-coated pulled-tip glass capillaries (20 nm i.d.) at a spray voltage of -
536 1000 V and a capillary temperature of 275°C. Spectra were acquired at a resolution of 50,000
537 at *m/z* 200, an AGC target between 5E4 and 1E5, and an RF lens of 60%. All MS1 and
538 MS/MS spectra were an average of 50 scans. The top 5 most abundant species were subjected
539 to higher energy collisional dissociation (HCD) for identification. MS/MS spectra were
540 obtained with an isolation width of 1 *m/z* and a normalized collision energy (NCE) ranging
541 from 22-26%.

542

543 **Liquid chromatography:** Lipids isolated from *Acinetobacter baumannii* were separated
544 using reversed-phase liquid chromatography (LC) on an Acquity UPLC CSH C18 column
545 (pore size 130 Å, 1.7 µm particle size, 2.1 mm × 100 mm, Waters) integrated with a Dionex

546 Ultimate 3000 UHPLC system (Thermo Fisher Scientific). Mobile phase A and B were
547 comprised of methanol: water: acetonitrile (3:4:3) and isopropanol: water: acetonitrile
548 (90:2.5:7.5), respectively, each containing 10 mM ammonium formate. Dried lipid content
549 from TLC bands was extracted via a Bligh and Dyer protocol and resuspended in 50:50
550 mobile phase (A: B) at a concentration of 100 ng/µL. A 9 µL injection volume was used, and
551 the column compartment was maintained at a temperature of 50 °C. Aminolipids were
552 separated at a flow rate of 0.275 mL/min with the following gradient: hold at 10% B (0-1
553 min), 10-45% B (1-5 min), 45-70% B (5-23 min), 70-95% B (23-24 min), hold at 95% B (24-
554 29 min), 95-10% B (29-29.5), and hold at 10% B (29.5-35 min).
555
556 **Untargeted LC-MS with HCD and Targeted LC-MS with UVPD Experiments:** An
557 untargeted negative-ionization mode LC-MS with HCD method was utilized to screen
558 *Acinetobacter baumannii* lipid extracts on a Thermo Scientific Orbitrap Fusion Lumos
559 Tribrid mass spectrometer via heated electrospray ionization. Various source parameters
560 included a spray voltage of -3800 V, sheath gas setting of 5, aux gas setting of 10, and
561 capillary temperature of 300 °C. MS1 data was collected at a resolution of 30,000 at *m/z* 200
562 in the Orbitrap analyzer with a scan range of *m/z* 500-1000, RF lens of 80%, and an AGC
563 target of 5E5. A data-dependent acquisition method was used where the top 5 most abundant
564 ions above an intensity threshold of 5E4 were selected for MS/MS analysis with HCD.
565 Species were isolated using a 1 *m/z* window and subjected to a collision energy corresponding
566 to NCE of 22%. MS/MS spectra were acquired at a resolution of 30,000 at *m/z* 200 in the
567 Orbitrap analyzer, AGC target of 1E5, maximum injection time of 250 ms, and 2
568 microscans/scan.

569 A targeted positive-ionization mode LC-MS/MS method was performed on a Thermo
570 Scientific Orbitrap Eclipse Tribrid mass spectrometer equipped with an ArF excimer laser
571 (Coherent, Inc.) for 193 nm ultraviolet photodissociation (UVPD). The heated electrospray
572 ionization source was operated at + 3800 V, and the source parameters described in the
573 untargeted experiments were implemented. MS/MS scans with UVPD were acquired in a
574 data-dependent manner, with 5 scans collected between each MS1 master scan, and with an
575 intensity threshold set at 5E4. A targeted mass filter was employed that included the *m/z*
576 values and start/end retention times for unsaturated aminolipids identified from the negative-
577 ionization mode LC-MS with HCD run (with a 15-ppm error tolerance). Aminolipids were
578 isolated with a 1 *m/z* window and activated with 4 laser pulses at 2 mJ/pulse for double bond
579 localization. MS/MS spectra were acquired at a resolution of 30,000 at *m/z* 200 in the
580 Orbitrap analyzer, q-value of 0.1, AGC target of 5E5, maximum injection time of 500 ms,
581 and 5 microscans/scan. Data was manually interpreted using Thermo Xcaliber Qual Browser
582 and ChemDraw. Precursor and fragment ions were assigned within 10 and 15 ppm mass
583 error, respectively.
584
585 **RNA sequencing.** Transcriptome sequencing analysis was performed as described
586 previously, with modification (53). Briefly, total RNA was extracted from *A. baumannii*
587 ATCC 17978 cultures grown in minimal medium supplemented with either excess (1 mM)
588 or limiting (50 μM) phosphate at OD_{600} of ~0.5 in triplicate, utilizing the Direct-Zol RNA
589 miniprep kit (Zymo Research). Genomic DNA contamination was eliminated using the
590 Turbo DNA-free DNA removal kit (Invitrogen). DNAase-treated RNA samples were then
591 forwarded to SeqCenter for sequencing on the Illumina NextSeq 550 sequencing.
592 Subsequently, the CLC Genomic Workbench software (Qiagen) was employed to map the

593 obtained sequencing data to the *A. baumannii* ATCC 17978 genome annotations and
594 determine the read per kilobase per million (RPKM) expression values and determine the
595 weighted-proportions fold changes in expression values between excess or limitation
596 phosphate conditions. Data were analyzed and plotted using GraphPad Prism software. Data
597 Accession #: GSE276010.
598
599 **Quantitative RT-PCR.** Relative-abundance quantitative PCR (qPCR) was performed as
600 previously described In brief, total RNA was extracted from bacterial cultures using the
601 Direct-Zol RNA Miniprep Kit (Zymo Research), followed by DNase digestion to remove
602 any genomic DNA. The RNA was then reverse transcribed into cDNA using the Invitrogen
603 SuperScript III Reverse Transcriptase (Thermo Fisher), with a final RNA concentration of 5
604 ng/µl. One microliter of the resulting cDNA was used as a template in a 10-µl quantitative
605 RT-PCR (qRT-PCR) reaction, conducted with Power SYBR Green Master Mix (Applied
606 Biosystems). qRT-PCR was carried out on a QuantStudio 3 Real-Time PCR System (Thermo
607 Fisher Scientific). Relative expression levels were calculated using the ΔΔCt method (56),
608 with normalization of gene targets to the *rpoA* signal.
609
610 **Microscopy and image analysis.** Cells were grown as stated above and fixed with
611 paraformaldehyde (PFA) and mounted on 1.5% agarose in 1X phosphate-buffered saline
612 (PBS). Imaging was performed using a Nikon Eclipse Ti-2 wide-field epifluorescence
613 microscope equipped with a Photometrics Prime 95B camera and a Plan Apo 100x, 1.45
614 numerical aperture objective lens. Images were captured using NIS Elements software.
615 Image analysis was conducted using the microbeJ plugin of ImageJ software.
616

617 **LOS staining and analysis.** All cultures were grown in test tubes containing 5 mL of
618 minimal medium with either excess (1 mM) or limiting (50 μM) phosphate at 37°C in a
619 shaker overnight. For the complementation strains, 30 μg/mL kanamycin and 1 mM IPTG
620 were added. The OD_{600} of the overnight cultures was measured and normalized to OD_{600} of
621 ~1. The cells were then centrifuged at 15,000 rpm for 5 minutes. Each pellet was resuspended
622 in 100 μl of 1X Sample Buffer (4X LDS Sample Buffer, 4% β-mercaptoethanol, and water)
623 and boiled in water for 10 minutes. After cooling, proteinase K was added to each sample
624 and mixed. The samples were then incubated in a 55°C water bath overnight. The following
625 day, the samples were boiled in water for 5 minutes and SDS-PAGE was performed. The gel
626 was then fixed and treated according to the protocol in the Pro-Q Emerald 300
627 Lipopolysaccharide Gel Stain Kit by Thermo Fisher Scientific (P20495).
628
629 **Colistin susceptibility assays.** Overnight cultures were diluted to OD_{600} ~0.150 in minimal
630 medium supplemented with either excess (1 mM) or limiting (50 μM) phosphate containing
631 5 mg/L colistin. Each culture, comprising 15 mL, was incubated in 125 mL Erlenmeyer flasks
632 at 37ºC with agitation at 250 rpm. Survivors were analyzed at specific time points by serial
633 dilution plating on LB agar.
634
635 **Funding**
636 The work was supported by funding from the National Institutes of Health (grants
637 R35GM143053 and R01AI168159 to J.M.B and R35GM139658 to J.S.B), and the Robert A.
638 Welch Foundation (F-1155 to J.S.B.). The funders had no role in study design, data collection
639 and analysis, decision to publish, or preparation of the manuscript.
640

641

642 **References**

643 1. Raetz CRH, Whitfield C. Lipopolysaccharide endotoxins. *Annu Rev Biochem.*
644 2002;71:635–700.
645 2. Sohlenkamp C, Geiger O. Bacterial membrane lipids: diversity in structures and
646 pathways. *FEMS Microbiol Rev.* 2016 Jan;40(1):133–59.
647 3. Geiger O, González-Silva N, López-Lara IM, Sohlenkamp C. Amino acid-containing
648 membrane lipids in bacteria. *Prog Lipid Res.* 2010 Jan;49(1):46–60.
649 4. Moore EK, Hopmans EC, Rijpstra WIC, Villanueva L, Damsté JSS. Elucidation and
650 identification of amino acid containing membrane lipids using liquid
651 chromatography/high-resolution mass spectrometry. *Rapid Commun Mass Spectrom*
652 RCM. 2016 Mar 30;30(6):739–50.
653 5. Vences-Guzmán MÁ, Geiger O, Sohlenkamp C. Ornithine lipids and their structural
654 modifications: from A to E and beyond. *FEMS Microbiol Lett.* 2012 Oct;335(1):1–10.
655 6. Geiger O, Röhrs V, Weissenmayer B, Finan TM, Thomas-Oates JE. The regulator gene
656 phoB mediates phosphate stress-controlled synthesis of the membrane lipid
657 diacylglyceryl-N,N,N-trimethylhomoserine in *Rhizobium (Sinorhizobium) meliloti. Mol*
658 *Microbiol.* 1999 Apr;32(1):63–73.
659 7. Dees C, Shively JM. Localization of quantitation of the ornithine lipid of *Thiobacillus*
660 *thiooxidans. J Bacteriol.* 1982 Feb;149(2):798–9.
661 8. Palacios-Chaves L, Conde-Álvarez R, Gil-Ramírez Y, Zúñiga-Ripa A, Barquero-Calvo
662 E, Chacón-Díaz C, et al. *Brucella abortus* ornithine lipids are dispensable outer
663 membrane components devoid of a marked pathogen-associated molecular pattern. *PloS*
664 *One.* 2011 Jan 7;6(1):e16030.

665 9. Vences-Guzmán MÁ, Guan Z, Ormeño-Orrillo E, González-Silva N, López-Lara IM,
666 Martínez-Romero E, et al. Hydroxylated ornithine lipids increase stress tolerance in
667 *Rhizobium tropici* CIAT899. *Mol Microbiol.* 2011 Mar;79(6):1496–514.
668 10. Stirrup R, Mausz MA, Silvano E, Murphy A, Guillonneau R, Quareshy M, et al.
669 Aminolipids elicit functional trade-offs between competitiveness and bacteriophage
670 attachment in *Ruegeria pomeroyi. ISME J.* 2023 Mar;17(3):315–25.
671 11. Weissenmayer B, Gao JL, López-Lara IM, Geiger O. Identification of a gene required
672 for the biosynthesis of ornithine-derived lipids. *Mol Microbiol.* 2002 Aug;45(3):721–33.
673 12. Gao JL, Weissenmayer B, Taylor AM, Thomas-Oates J, López-Lara IM, Geiger O.
674 Identification of a gene required for the formation of lyso-ornithine lipid, an intermediate
675 in the biosynthesis of ornithine-containing lipids. *Mol Microbiol.* 2004 Sep;53(6):1757–
676 70.
677 13. Vences-Guzmán MÁ, Guan Z, Escobedo-Hinojosa WI, Bermúdez-Barrientos JR, Geiger
678 O, Sohlenkamp C. Discovery of a bifunctional acyltransferase responsible for ornithine
679 lipid synthesis in *Serratia proteamaculans. Environ Microbiol.* 2015 May;17(5):1487–
680 96.
681 14. Lewenza S, Falsafi R, Bains M, Rohs P, Stupak J, Sprott GD, et al. The *olsA* gene
682 mediates the synthesis of an ornithine lipid in *Pseudomonas aeruginosa* during growth
683 under phosphate-limiting conditions, but is not involved in antimicrobial peptide
684 susceptibility. *FEMS Microbiol Lett.* 2011 Jul;320(2):95–102.
685 15. Barbosa LC, Goulart CL, Avellar MM, Bisch PM, von Kruger WMA. Accumulation of
686 ornithine lipids in *Vibrio cholerae* under phosphate deprivation is dependent on VC0489
687 (OlsF) and PhoBR system. *Microbiol Read Engl.* 2018 Mar;164(3):395–9.

688 16. Harding CM, Hennon SW, Feldman MF. Uncovering the mechanisms of *Acinetobacter*
689 *baumannii* virulence. *Nat Rev Microbiol.* 2018 Feb;16(2):91–102.
690 17. Rojas-Jiménez K, Sohlenkamp C, Geiger O, Martínez-Romero E, Werner D, Vinuesa P.
691 A ClC chloride channel homolog and ornithine-containing membrane lipids of
692 *Rhizobium tropici* CIAT899 are involved in symbiotic efficiency and acid tolerance. *Mol*
693 *Plant-Microbe Interact MPMI.* 2005 Nov;18(11):1175–85.
694 18. González-Silva N, López-Lara IM, Reyes-Lamothe R, Taylor AM, Sumpton D, Thomas-
695 Oates J, et al. The dioxygenase-encoding *olsD* gene from *Burkholderia cenocepacia*
696 causes the hydroxylation of the amide-linked fatty acyl moiety of ornithine-containing
697 membrane lipids. *Biochemistry.* 2011 Jul 26;50(29):6396–408.
698 19. Boll JM, Tucker AT, Klein DR, Beltran AM, Brodbelt JS, Davies BW, et al. Reinforcing
699 Lipid A Acylation on the Cell Surface of *Acinetobacter baumannii* Promotes Cationic
700 Antimicrobial Peptide Resistance and Desiccation Survival. *mBio.* 2015;6(3):e00478-
701 00415.
702 20. Boll JM, Crofts AA, Peters K, Cattoir V, Vollmer W, Davies BW, et al. A penicillin-
703 binding protein inhibits selection of colistin-resistant, lipooligosaccharide-deficient
704 *Acinetobacter baumannii. Proc Natl Acad Sci U S A.* 2016 11;113(41):E6228–37.
705 21. Kang KN, Klein DR, Kazi MI, Guérin F, Cattoir V, Brodbelt JS, et al. Colistin
706 heteroresistance in *Enterobacter cloacae* is regulated by PhoPQ-dependent 4-amino-4-
707 deoxy-l-arabinose addition to lipid A. *Mol Microbiol.* 2019;111(6):1604–16.
708 22. Murtha AN, Kazi MI, Schargel RD, Cross T, Fihn C, Cattoir V, et al. High-level
709 carbapenem tolerance requires antibiotic-induced outer membrane modifications. *PLoS*
710 *Pathog.* 2022 Feb;18(2):e1010307.

711 23. Ernst CM, Peschel A. Broad-spectrum antimicrobial peptide resistance by MprF-
712 mediated aminoacylation and flipping of phospholipids. *Mol Microbiol.* 2011
713 Apr;80(2):290–9.
714 24. Needham BD, Trent MS. Fortifying the barrier: the impact of lipid A remodelling on
715 bacterial pathogenesis. *Nat Rev Microbiol.* 2013 Jul;11(7):467–81.
716 25. Henderson JC, Zimmerman SM, Crofts AA, Boll JM, Kuhns LG, Herrera CM, et al. The
717 Power of Asymmetry: Architecture and Assembly of the Gram-Negative Outer
718 Membrane Lipid Bilayer. *Annu Rev Microbiol.* 2016 08;70:255–78.
719 26. de Rudder KE, Thomas-Oates JE, Geiger O. Rhizobium meliloti mutants deficient in
720 phospholipid N-methyltransferase still contain phosphatidylcholine. *J Bacteriol.* 1997
721 Nov;179(22):6921–8.
722 27. Kamischke C, Fan J, Bergeron J, Kulasekara HD, Dalebroux ZD, Burrell A, et al. The
723 Acinetobacter baumannii Mla system and glycerophospholipid transport to the outer
724 membrane. *eLife.* 2019 14;8.
725 28. Raetz CR, Dowhan W. Biosynthesis and function of phospholipids in *Escherichia coli.*
726 *J Biol Chem.* 1990 Jan 25;265(3):1235–8.
727 29. Lopalco P, Stahl J, Annese C, Averhoff B, Corcelli A. Identification of unique cardiolipin
728 and monolysocardiolipin species in *Acinetobacter baumannii. Sci Rep.* 2017 Jun
729 7;7(1):2972.
730 30. Smith AF, Rihtman B, Stirrup R, Silvano E, Mausz MA, Scanlan DJ, et al. Elucidation
731 of glutamine lipid biosynthesis in marine bacteria reveals its importance under
732 phosphorus deplete growth in *Rhodobacteraceae. ISME J.* 2019 Jan;13(1):39–49.

733 31. Jones RA, Shropshire H, Zhao C, Murphy A, Lidbury I, Wei T, et al. Phosphorus stress
734 induces the synthesis of novel glycolipids in *Pseudomonas aeruginosa* that confer
735 protection against a last-resort antibiotic. *ISME J.* 2021 Nov;15(11):3303–14.
736 32. Stankeviciute G, Guan Z, Goldfine H, Klein EA. *Caulobacter crescentus* Adapts to
737 Phosphate Starvation by Synthesizing Anionic Glycoglycerolipids and a Novel
738 Glycosphingolipid. *mBio. 2*019 Apr 2;10(2):e00107-19.
739 33. Escobedo-Hinojosa WI, Vences-Guzmán MÁ, Schubotz F, Sandoval-Calderón M,
740 Summons RE, López-Lara IM, et al. OlsG (Sinac_1600) Is an Ornithine Lipid N-
741 Methyltransferase from the Planctomycete *Singulisphaera acidiphila. J Biol Chem.* 2015
742 Jun 12;290(24):15102–11.
743 34. Kim SK, Park SJ, Li XH, Choi YS, Im DS, Lee JH. Bacterial ornithine lipid, a surrogate
744 membrane lipid under phosphate-limiting conditions, plays important roles in bacterial
745 persistence and interaction with host. *Environ Microbiol.* 2018 Nov;20(11):3992–4008.
746 35. Gallagher LA, Ramage E, Weiss EJ, Radey M, Hayden HS, Held KG, et al. Resources
747 for Genetic and Genomic Analysis of Emerging Pathogen *Acinetobacter baumannii. J*
748 *Bacteriol.* 2015 Jun 15;197(12):2027–35.
749 36. Hebecker S, Arendt W, Heinemann IU, Tiefenau JHJ, Nimtz M, Rohde M, et al. Alanyl-
750 phosphatidylglycerol synthase: mechanism of substrate recognition during tRNA-
751 dependent lipid modification in *Pseudomonas aeruginosa. Mol Microbiol.* 2011
752 May;80(4):935–50.
753 37. Arendt W, Hebecker S, Jäger S, Nimtz M, Moser J. Resistance phenotypes mediated by
754 aminoacyl-phosphatidylglycerol synthases. *J Bacteriol.* 2012 Mar;194(6):1401–16.
755 38. Baek JH, Lee SY. Novel gene members in the Pho regulon of *Escherichia coli. FEMS*
756 *Microbiol Lett.* 2006 Nov;264(1):104–9.

757 39. Hsieh YJ, Wanner BL. Global regulation by the seven-component Pi signaling system.
758 *Curr Opin Microbiol.* 2010 Apr;13(2):198–203.
759 40. Gardner SG, McCleary WR. Control of the phoBR Regulon in *Escherichia coli. EcoSal*
760 Plus. 2019 Sep;8(2).
761 41. Hankins JV, Madsen JA, Giles DK, Brodbelt JS, Trent MS. Amino acid addition to
762 Vibrio cholerae LPS establishes a link between surface remodeling in gram-positive and
763 gram-negative bacteria. *Proc Natl Acad Sci U S A.* 2012 May 29;109(22):8722–7.
764 42. Sohlenkamp C, Galindo-Lagunas KA, Guan Z, Vinuesa P, Robinson S, Thomas-Oates J,
765 et al. The lipid lysyl-phosphatidylglycerol is present in membranes of *Rhizobium tropici*
766 CIAT899 and confers increased resistance to polymyxin B under acidic growth
767 conditions. *Mol Plant-Microbe Interact MPMI.* 2007 Nov;20(11):1421–30.
768 43. Klein S, Lorenzo C, Hoffmann S, Walther JM, Storbeck S, Piekarski T, et al. Adaptation
769 of *Pseudomonas aeruginosa* to various conditions includes tRNA-dependent formation
770 of alanyl-phosphatidylglycerol. *Mol Microbiol.* 2009 Feb;71(3):551–65.
771 44. Ernst CM, Staubitz P, Mishra NN, Yang SJ, Hornig G, Kalbacher H, et al. The bacterial
772 defensin resistance protein MprF consists of separable domains for lipid lysinylation and
773 antimicrobial peptide repulsion. *PLoS Pathog.* 2009 Nov;5(11):e1000660.
774 45. Geiger O, Padilla-Gómez J, López-Lara IM. Bacterial Sphingolipids and Sulfonolipids.
775 In: Geiger O, editor. Biogenesis of Fatty Acids, Lipids and Membranes [Internet]. Cham:
776 Springer International Publishing; 2019 [cited 2024 Jul 2]. p. 123–37. Available from:
777 https://doi.org/10.1007/978-3-319-50430-8_12
778 46. Zhang X, Ferguson-Miller SM, Reid GE. Characterization of ornithine and glutamine
779 lipids extracted from cell membranes of *Rhodobacter sphaeroides. J Am Soc Mass*
780 *Spectrom.* 2009 Feb;20(2):198–212.

781 47. Aygun-Sunar S, Bilaloglu R, Goldfine H, Daldal F. *Rhodobacter capsulatus* OlsA is a
782 bifunctional enzyme active in both ornithine lipid and phosphatidic acid biosynthesis. *J*
783 *Bacteriol.* 2007 Dec;189(23):8564–74.
784 48. Wijers CDM, Pham L, Menon S, Boyd KL, Noel HR, Skaar EP, et al. Identification of
785 Two Variants of *Acinetobacter baumannii* Strain ATCC 17978 with Distinct Genotypes
786 and Phenotypes. *Infect Immun.* 2021 Nov 16;89(12):e0045421.
787 49. Tipton KA, Dimitrova D, Rather PN. Phase-Variable Control of Multiple Phenotypes in
788 *Acinetobacter baumannii* Strain AB5075. *J Bacteriol.* 2015 Jul 6;197(15):2593–9.
789 50. Tucker AT, Nowicki EM, Boll JM, Knauf GA, Burdis NC, Trent MS, et al. Defining
790 gene-phenotype relationships in *Acinetobacter baumannii* through one-step
791 chromosomal gene inactivation. *mBio.* 2014;5(4):e01313-01314.
792 51. Kang KN, Kazi MI, Biboy J, Gray J, Bovermann H, Ausman J, et al. Septal Class A
793 Penicillin-Binding Protein Activity and ld-Transpeptidases Mediate Selection of
794 Colistin-Resistant Lipooligosaccharide-Deficient *Acinetobacter baumannii. mBio.* 2021
795 Jan 5;12(1):e02185-20.
796 52. Kang KN, Boll JM. PBP1A Directly Interacts with the Divisome Complex to Promote
797 Septal Peptidoglycan Synthesis in *Acinetobacter baumannii. J Bacteriol.* 2022 Dec
798 20;204(12):e0023922.
799 53. Islam N, Kazi MI, Kang KN, Biboy J, Gray J, Ahmed F, et al. Peptidoglycan Recycling
800 Promotes Outer Membrane Integrity and Carbapenem Tolerance in *Acinetobacter*
801 *baumannii. mBio.* 2022 Jun 28;13(3):e0100122.
802 54. Podolsky T, Fong ST, Lee BT. Direct selection of tetracycline-sensitive *Escherichia coli*
803 cells using nickel salts. *Plasmid.* 1996 Sep;36(2):112–5.

804 55. Bligh EG, Dyer WJ. A rapid method of total lipid extraction and purification. C*an J*
805 *Biochem Physiol.* 1959 Aug;37(8):911–7.
806 56. Livak KJ, Schmittgen TD. Analysis of relative gene expression data using real-time
807 quantitative PCR and the 2(-Delta Delta C(T)) *Method.* Methods San Diego Calif. 2001
808 Dec;25(4):402–8.

809
810
811
812
813
814
815
816
817
818
819
820
821

822 **Figures**

823
824
825
826
827
828
829
830
831

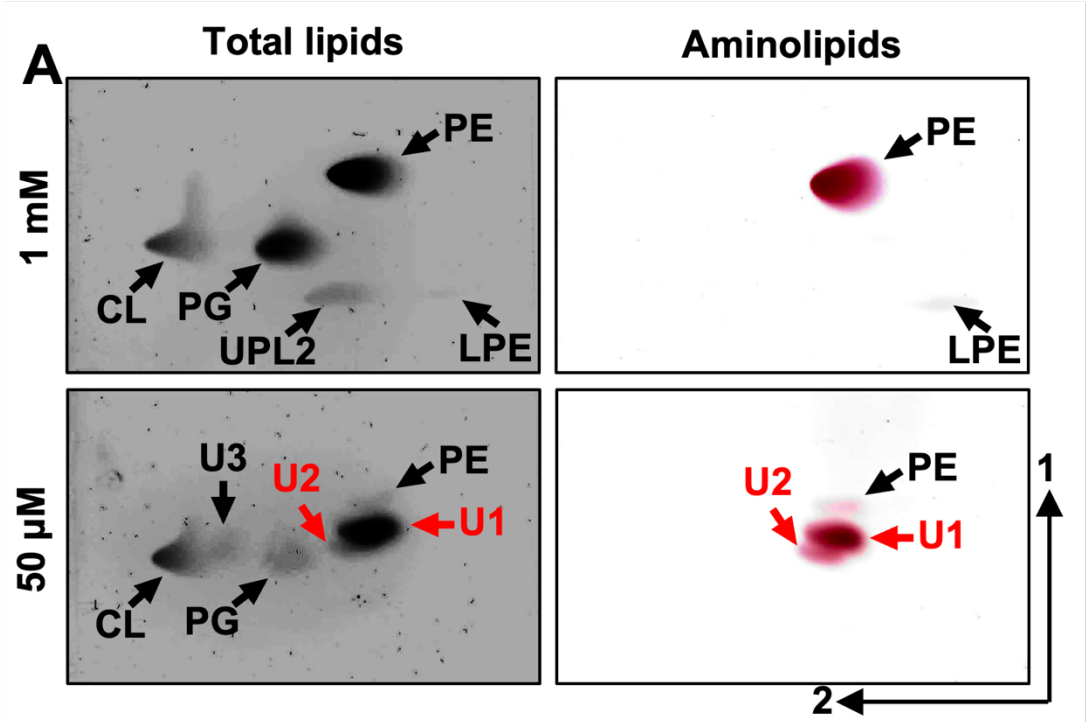

Figure 1: Lipid composition of *A. baumannii* strain ATCC 17978 in excess and limiting phosphate concentrations. A. Strains were grown in basal media 2 (BM2) with excess (1mM) or limiting (50 µM) phosphate. Cells were collected, lipids were extracted using the Bligh and Dyer method and separated using 2-dimensional thin-layer chromatography. Total lipids were stained with sulfuric acid (left). Aminolipids were stained using ninhydrin (right). Specific lipids are labelled: PE, phosphatidylethanolamine; PG, phosphatidylglycerol; CL, cardiolipin; LPE, lyso-PE; U1, unknown lipid 1; U2, unknown lipid 2; UPL1, unknown phospholipid 1. Red letters denote aminolipids that provide the focus of the study.

832
833
834
835
836
837
838

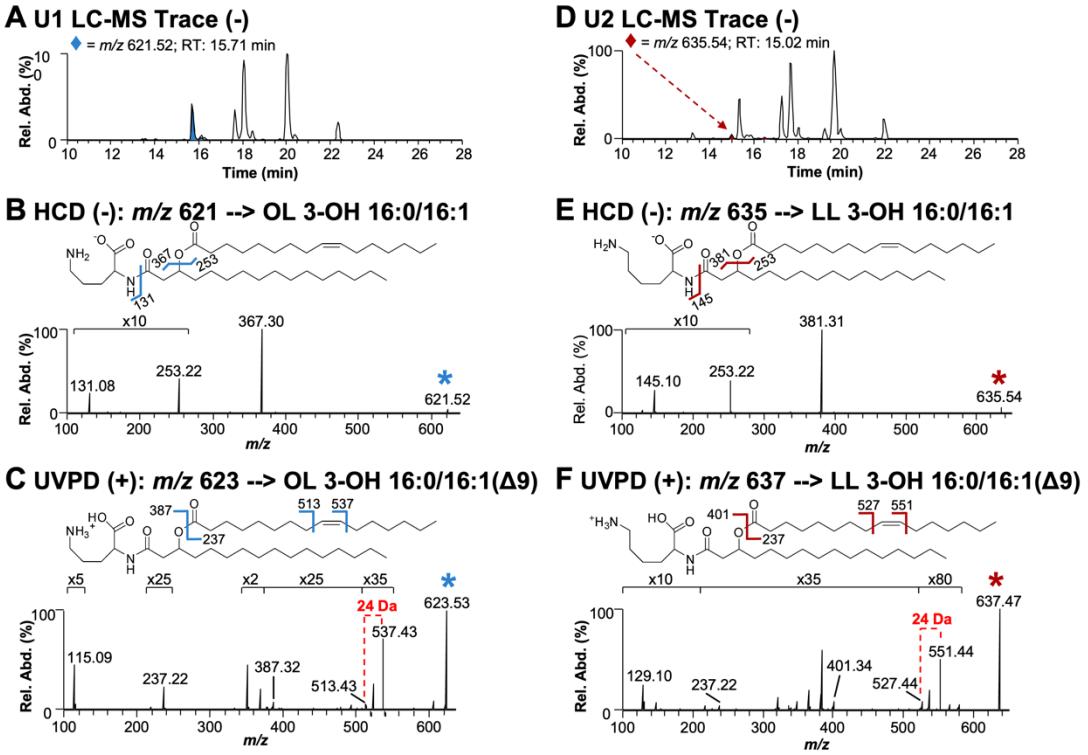

Figure 2: Structural analysis of the lipids produced during phosphate limitation. A. LC-MS trace of U1 lipid extract in negative-ionization mode. **B.** HCD (NCE 22) mass spectrum of *m/z* 621.52 ($[M-H]^-$), an ornithine lipid found in the U1 extract**. C.** UVPD (4 pulses at 2 mJ/pulse) mass spectrum of *m/z* 623.53 ($[M+H]^+$). **D.** LC-MS trace of U2 lipid extract in negative-ionization mode. **E.** HCD (NCE 22) mass spectrum of *m/z* 635.54 ($[M-H]^-$), a lysine lipid found in U2 extract. **F.** UVPD (4 pulses at 2 mJ/pulse) mass spectrum of *m/z* 637.47 ($[M+H]^+$). The selected precursor ions are labeled with asterisks in B, C, E, and F.

845

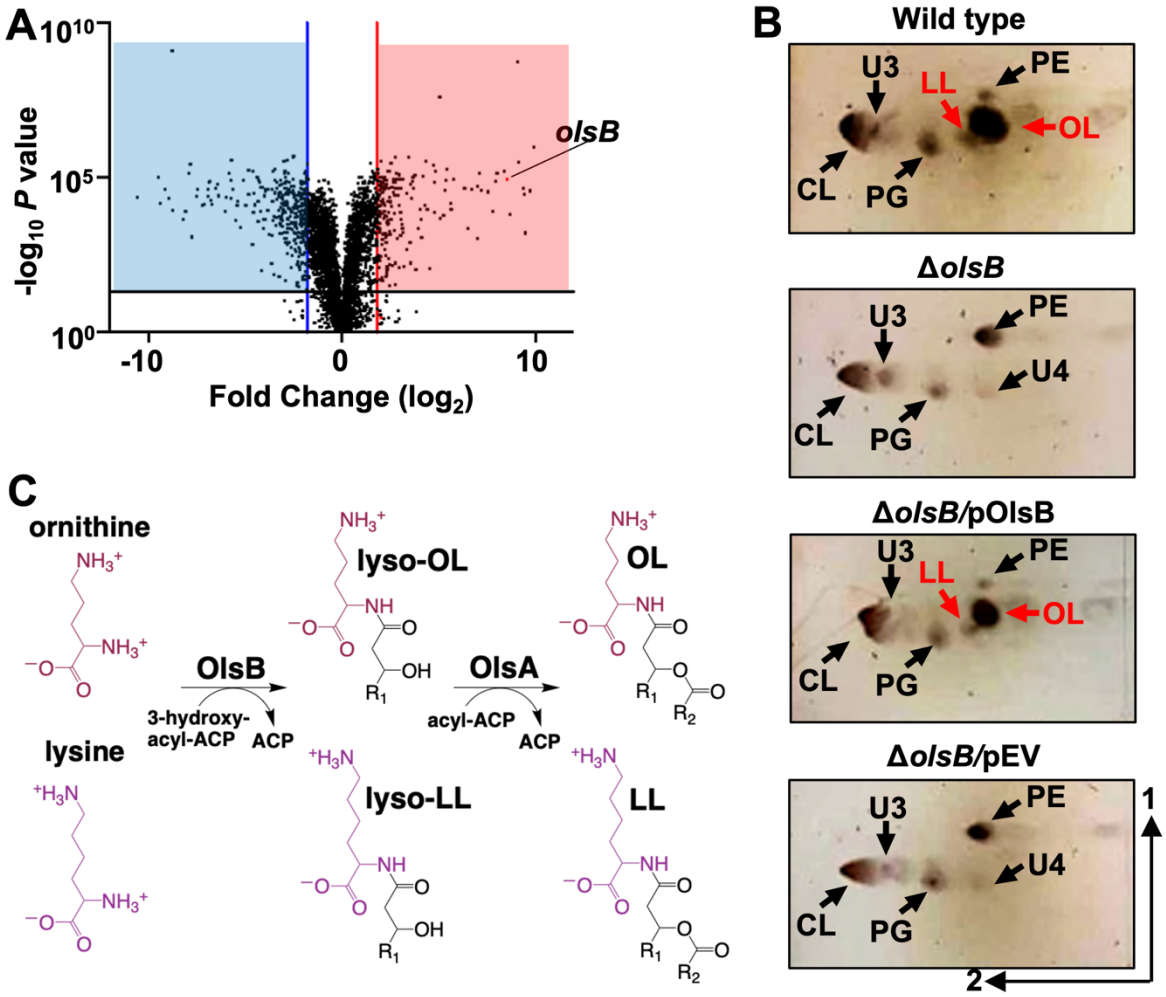

Figure 3: The *olsB* gene is required for ornithine and lysine lipid formation in phosphate limited growth conditions. A. Volcano plot of differentially regulated genes in excess and limiting phosphate. Lines indicate 3.5-fold cutoffs. **B.** 2D thin-layer chromatography stained with sulfuric acid showing wild type and Δ*olsB* strains grown in phosphate limiting (50 µM) conditions. Specific lipids are labelled: PE, phosphatidylethanolamine; PG, phosphatidylglycerol; CL, cardiolipin; OL, ornithine lipid; LL, lysine lipid; U3, unknown lipid 3; U4, unknown lipid 4. OL and LL aminolipids are labelled in red. **C.** Proposed ornithine lipid (OL) and lysine lipid (LL) biosynthesis pathways in *A. baumannii*.

846

847

848

849

850

851

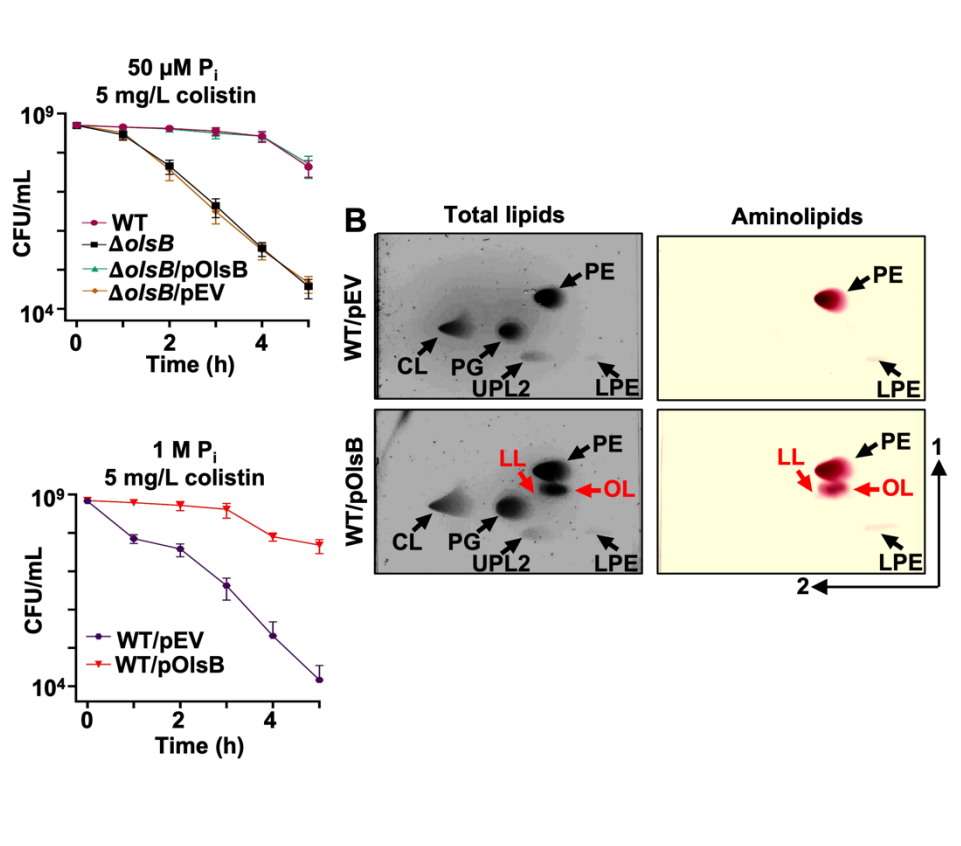

Figure 4: Aminolipids promote colistin tolerance in *A. baumannii*. A. Colistin-dependent killing in wild type and Δ*olsB* mutant strains under phosphate limitation ($n = 3$). Error bars indicate standard deviation. Wild type (WT) strains carrying pOlsB or empty vector were subjected to 5 mg/L colistin exposure over time. CFU/mL were calculated every 0.5 h. **B.** Total lipids were extracted using the Bligh and Dyer method and separated using 2D thin-layer chromatography. Lipids were stained with sulfuric acid (left). Aminolipids were stained using ninhydrin (right). Specific lipids are labelled: PE, phosphatidylethanolamine; PG, phosphatidylglycerol; CL, cardiolipin; LPE, lyso-phosphatidylethanolamine; LL, lysine lipid; OL, ornithine lipid; U3, unknown lipid 3. OL and LL are labelled in red. **C.** Colistin-dependent kill curves (left) and growth rate analysis (right) in wild type expressing empty vector (pEV) or pOlsB under high phosphate conditions ($n = 3$). Error bars indicate standard deviation.

863

864

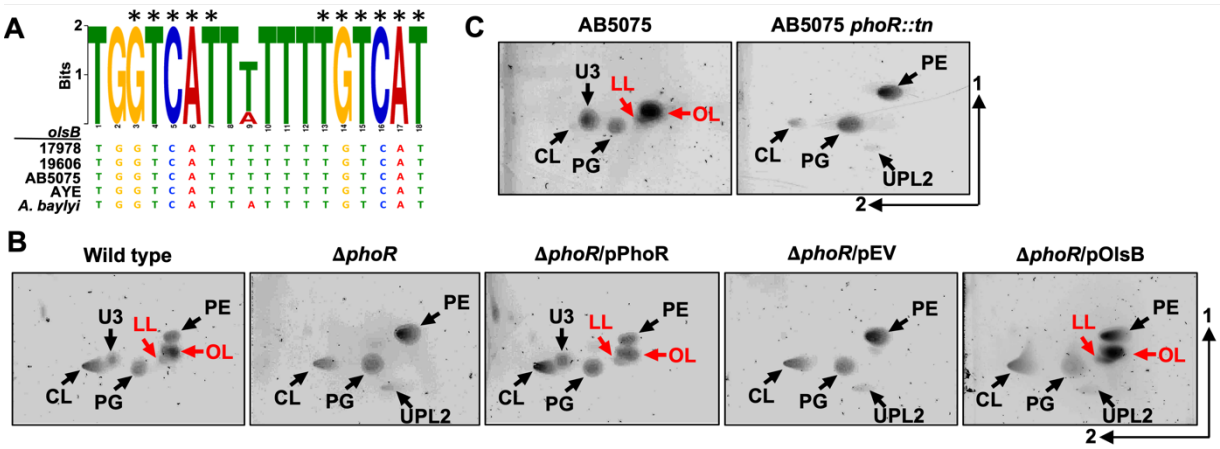

Figure 5: PhoR regulates *olsB* gene expression and aminolipid formation in *A. baumannii* strains. **A.** Predicted Pho box sequence alignments from *A. baumannii* strain 17978, 19606, AB5075, AYE, and *A. baylyi olsB* promoters. Black asterisks represent conserved nucleotides in the *E. coli* Pho box consensus (CT*GTCAT*NNNNC*TGTCAT*). **B.** 2D thin-layer chromatography lipid analysis from *A. baumannii* strain ATCC 17978 wild type and mutants grown in minimal media supplemented with 50 µM (limiting) phosphate. **C.** 2D thin-layer chromatography lipid analysis from *A. baumannii* strain AB5075 wild type and the *phoR* Tn*26* mutant in minimal media supplemented with 50 µM (limiting) phosphate. Lipids were stained with sulfuric acid. OL and LL aminolipids are labelled in red.

865

866

867

868

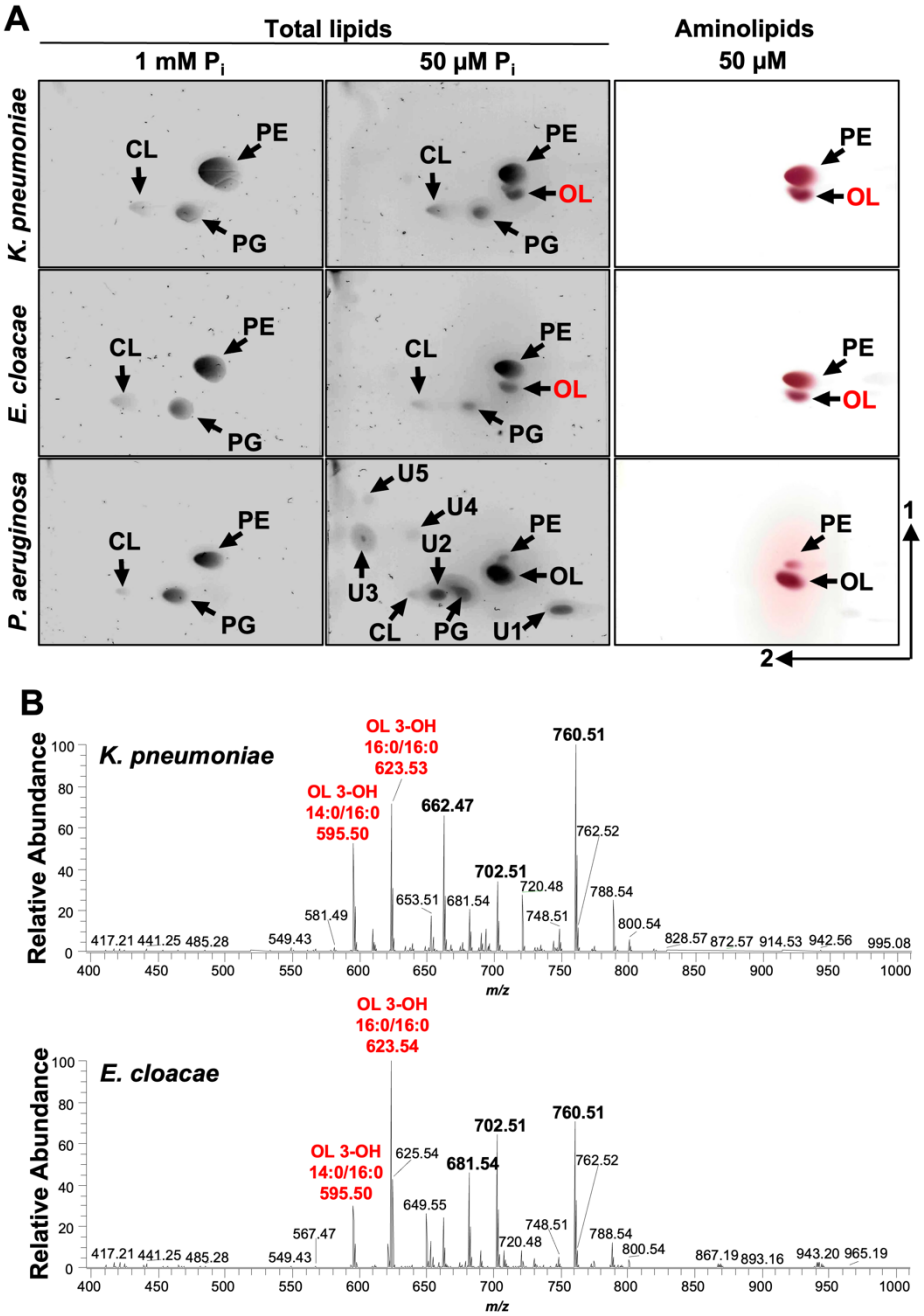

Figure 6: Aminolipid biosynthesis is conserved in Gram-negative ESKAPE pathogens. 2D thin-layer chromatography of lipids extracted from wild type *K. pneumoniae* strain KPNIH1, *E. cloacae* strain ATCC 13047, and *P. aeruginosa* strain PAO1 grown in excess (1 mM) or limiting (50 μM) phosphate conditions. Totals lipids were stained with sulfuric acid (left). Aminolipids were stained using ninhydrin (right). Specific lipids are labelled: PE, phosphatidylethanolamine; PG, phosphatidylglycerol; CL, cardiolipin; OL, ornithine lipid; U1, U2, U3, U4, and U5; unknown compounds 1, 2, 3, 4, and 5. **B.** Representative MS1 spectra from shotgun analysis of animolipids isolated from *K. pneumoniae* (n = 3) and *E. cloacae* (n = 3). The five most enriched lipids are bolded, including two ornithine lipids (OL), labelled in red.

888 **Supplementary Captions**

889 **Figure S1: *Escherichia coli* (*Ec*) and *Acinetobacter baumannii (Ab)* lipid composition**
890 **after growth in complex media. A.** Strains were grown in complex media (LB broth) in the
891 presence of ^{32}P-orthopohosphoric acid until mid-logarithmic growth phase. Cells were
892 collected and total lipids were extracted using the Bligh and Dyer method and separated using
893 2-dimensional thin-layer chromatography. Labelled lipids include anionic cardiolipin (CL)
894 and phosphatidylglycerol (PG), aminolipids phosphatidylethanolamine (PE) and lyso-PE
895 (LPE), and unknown phospholipid 1 (UPL1). **B.** PG, PE, CL and LPE chemical structures.
896 Head groups are red, the glycerol backbone is blue, and fatty acids are black.

897

898 **Figure S2: Effect of phosphate availability on growth, cell morphology, and LOS**
899 **production. A.** Quantification of total lipid in TLC (A) grown in excess or limiting
900 phosphate concentrations. Lipids are graphed as a percentage of the total. Significance testing
901 conducted using Student *t* test with two-tailed distribution assuming equal variance. Lines
902 indicate standard deviation. *$P < 0.05$; ns is not significant. **B.** *A. baumannii* ATCC 17978
903 was cultured in minimal medium containing either excess (1 mM) or limiting (50 μM)
904 phosphate for 24 hours. **C.** Phase-contrast images of *A. baumannii* grown under these
905 conditions, captured during the exponential phase. Scalebar is 10 μm. **D.** Cell length and area
906 were quantified for each population ($n \geq 150$) using ImageJ software. Each point represents
907 an individual cell. The experiment was repeated twice, and one representative dataset was
908 reported. Significance testing conducted using Student *t* test with two-tailed distribution
909 assuming equal variance. ***$P < 0.001$, ****$P < 0.0001$. **E.** Proteinase K-treated whole-cell
910 lysate from wild-type *A. baumannii* strains ATCC 17978, ATCC 19606, and AB5075, as
911 well as from aminolipid-deficient mutants grown under excess (1mM) or limiting (50 μM)

912 phosphate conditions. The LOS samples were separated using SDS-PAGE and stained using
913 Pro-Q Emerald 300.
914
915 **Figure S3: Thin-layer chromatography of *Acinetobacter* aminolipids. A.** To produce *A.*
916 *baumannii* lipid samples for MS analysis, total lipids were separated using thin-layer
917 chromatography and scraped from the plate, extracted using the Bligh and Dyer method, and
918 run alongside lipid controls. Extractions resulted in isolation of U1 & U2, U1, or U2. Lipids
919 were stained with ninhydrin to visualize aminolipids. Specific lipids are labelled: PE,
920 phosphatidylethanolamine; U1, unknown lipid 1; U2, unknown lipid 2. **B.** Cells were grown
921 in minimal medium supplemented with excess (1mM) or limiting (50 μM) phosphate
922 conditions from indicated *Acinetobacter* strains. Total lipids were extracted from cells grown
923 in media with limiting phosphate concentrations. Total lipids were spotted on thin-layer
924 chromatography and separated based on hydrophobicity. Plates were stained with ninhydrin
925 to visualize aminolipids. Specific lipids are labelled: PE, phosphatidylethanolamine; OL,
926 ornithine lipid; LL, lysine lipid. **C.** To produce *E. cloacae* and *K. pneumoniae* samples for
927 MS analysis, total lipids were extracted from cells grown in media with limiting phosphate
928 concentrations. Total lipids were separated using thin-layer chromatography and scraped
929 from the plate, extracted using the Bligh and Dyer method, and run alongside lipid controls.
930 Lipids were stained with ninhydrin to visualize aminolipids. Specific lipids are labelled: PE,
931 phosphatidylethanolamine; OL; ornithine lipid (predicted).
932
933 **Figure S4: *olsB* and *olsA* are required for ornithine and lysine lipid biosynthesis in *A.***
934 ***baumannii.* A.** Relative-abundance quantitative PCR (qPCR) of genes after *A. baumannii*
935 growth in excess or limiting phosphate concentrations (n = 3). Lines indicate standard

936 deviation. Significance testing was conducted using Student *t* test with two-tailed distribution
937 assuming equal variance**.** *$P < 0.05$; ns = not significant. **B.** 2D thin-layer chromatography
938 lipid analysis in ATCC 19606 wild type and the Δ*olsB* mutant strain after growth in limiting
939 (50 μM) phosphate concentrations. Lipids were stained with sulfuric acid. **C.** Analysis in
940 AB5075 wild type and transposon (Tn*101*) mutant strains after growth in limiting (50 μM)
941 phosphate concentrations. Specific lipids are labelled: PE, phosphatidylethanolamine; PG,
942 phosphatidylglycerol; CL, cardiolipin; OL, ornithine lipid; LL, lysine lipid. OL and LL
943 aminolipids are labelled in red. **D.** Phase-contrast images of *A. baumannii* strain ATCC
944 17978 grown under phosphate limiting conditions, captured during exponential phase
945 growth. Scalebar is 10 μm. **E.** Cell length and area of strain ATCC 17978 were quantified
946 for each population ($n \geq 150$) using ImageJ software. Each point represents an individual
947 cell. Significance testing was conducted using Student *t* test with two-tailed distribution
948 assuming equal variance. ns = not significant. **F**. Optical density (OD_{600}) measurements of
949 *A. baumannii* strains grown in 50 μM phosphate over 24 h.
950
951 **Figure S5: Aminolipid formation promotes *A. baumannii* tolerance to colistin.** Growth
952 (OD_{600}) of *A. baumannii* ATCC 17978 strains was measured at 37 °C in minimal medium
953 with limiting phosphate (**A**) or excess phosphate (**B**), and in the presence of colistin at
954 concentrations of 1, 2.5, or 5 mg/L.
955
956 **Figure S6: Thin-layer chromatography of *E. cloacae* and *K. pneumoniae* aminolipids.**
957 To produce *E. cloacae* and *K. pneumoniae* samples for MS analysis, total lipids were
958 extracted from cells grown in media with limiting phosphate concentrations. Total lipids were
959 separated using thin-layer chromatography and scraped from the plate, extracted using the

960 Bligh and Dyer method, and run alongside lipid controls. Lipids were stained with ninhydrin
961 to visualize aminolipids. Specific lipids are labelled: PE, phosphatidylethanolamine; OL;
962 ornithine lipid (predicted).
963
964 **Table S1: Identity of aminolipids in unknown lipid 1 biological replicates.**
965
966 **Table S2: Identity of aminolipids in unknown lipid 2 (U2) biological replicates.**
967
968 **Table S3: Differentially regulated genes in excess and limiting phosphate**
969
970 **Table S4: Lipids present in the top five most abundant species from *K. pneumoniae***
971 **biological replicates**
972
973 **Table S5: Lipids present in the top five most abundant species from *E. cloacae* biological**
974 **replicates**
975
976 **Table S6: Strains and plasmids used in this study.**
977
978 **Table S7: Primers used in this study.**
979